https://doi.org/10.5194/egusphere-2026-3061
Preprint. Discussion started: 11 June 2026

Multi-Sensor Remote Sensing Evidence of Connection between Deep Aquifer Recharge in California's Central Valley and Sierra Nevada Snowmelt

Susanna Werth[1,2], Manoochehr Shirzaei[1,2,3], Grace Carlson[1,4], and Roland Bürgmann[5]

[1]Virginia Tech, Department of Geosciences, Blacksburg, VA, USA.
[2]Virginia Tech, National Security Institute, Blacksburg, VA, USA.
[3]United Nations University, Institute for Water, Environment and Health, Hamilton, ON L8P 0A1, Canada
[4]Indiana University, Department of Geography, Bloomington, IN, USA
[5]University of California, Berkeley, Department of Earth and Planetary Science, Berkeley, CA, USA.

Correspondence to: Susanna Werth (swerth@vt.edu)

Abstract.

California's arid Central Valley (CV) relies heavily on groundwater extracted from deep aquifers (>50 m) and imported surface water to sustain approximately one-quarter of the United States' food production. While the recharge to deep aquifers in CV is hypothesized to be influenced by hydrologic processes in the adjacent Sierra Nevada, direct observational evidence at regional scales remains limited.

Here, we present an integrated analysis of multi-decadal geodetic remote sensing, hydrologic, and climate datasets, including groundwater levels, GRACE-derived water storage, GNSS and InSAR deformation, and snowmelt observations, to investigate the spatiotemporal relationships between mountain hydrology and deep aquifer dynamics in the CV. A consistent sequence of seasonal signals emerges across independent datasets: peak groundwater levels in deep CV aquifers occur approximately one month after peak water availability from Sierra Nevada snowmelt, while peak groundwater storage inferred from GRACE lags groundwater levels by approximately three months.

These phase delays indicate that groundwater systems respond to mountain hydrologic forcing through temporally distinct processes, with pressure signals propagating more rapidly than changes in bulk water storage. A simplified first-order diffusion analysis shows that the observed lag between snowmelt and the groundwater-level response is feasible, given plausible pressure propagation timescales in fractured mountain bedrock.

Together, these results provide observational evidence consistent with a hydraulic connection between high-mountain aquifers and deep basin aquifers via mountain block recharge (MBR). Our findings highlight the importance of incorporating mountain-driven recharge processes and pressure dynamics into regional hydroclimate models and groundwater management strategies, particularly in snowmelt-dominated and water-stressed regions.

https://doi.org/10.5194/egusphere-2026-3061
Preprint. Discussion started: 11 June 2026

1 Introduction

The global availability of groundwater is threatened by over-extraction and climate variability, particularly in semi-arid agricultural regions, where groundwater provides a critical buffer during droughts and dry growing seasons (Jasechko et al., 2024; Madani, 2026; WMO, 2025). A key challenge in such systems is that groundwater demand is often met by deeper, semi-confined aquifers, whereas recharge through natural percolation or managed aquifer recharge (MAR) is more readily connected to shallow, unconfined aquifers. A direct consequence of deeper confined aquifers is land subsidence, which can lead to fissure generation, sinkholes, infrastructure damage, and accelerate relative sea-level rise (Galloway et al., 2000; Herrera-García et al., 2021). Hence, understanding both natural and artificial processes that replenish aquifers is essential for sustainable water management, hazard prevention, and water storage for future use (Escriva-Bou et al., 2020, 2021; Ghasemizade et al., 2019).

California's Central Valley (CV) is a prominent example of this challenge. During a dry year, up to 70% of the groundwater used in the CV is pumped within the growing season, mainly between April and June (Faunt, 2009), causing a long-term decline in groundwater levels, with the fastest rates observed in the southern San Joaquin basin, including the Tulare basin (Fig. 1a) (Faunt, 2009; Faunt et al., 2016; Konikow, 2015; Massoud et al., 2018; Ojha et al., 2018). Given the poor quality of shallow water in the southern CV (Hanak et al., 2017), most groundwater demand is met by tapping deep aquifers at depths of ~50 m to ~500 m below the surface (see Fig. 1b in Perrone & Jasechko, 2019). These aquifers are overlain by the confining layer of the Corcoran Clay and widespread clay lenses (Faunt, 2009) (Fig. 1a, 2). Although the clay lenses are discontinuous, taken together, they significantly reduce vertical hydraulic conductivity (Faunt, 2009).

This hydrogeologic setting limits the direct connection between surface-water availability and recharge of the deeper aquifer system. Recharge via direct percolation or diffuse fluxes of surface water vertically into several-hundred-meters-deep (semi-) confined aquifers of the CV through the impermeable Corcoran Clay layer or clay lenses is implausible, at least at the time scale of a month to a year (Shirzaei et al., 2019), corroborated by groundwater-age data (McMahon et al., 2011). For instance, Burow et al. (2007) reported a recharge rate of less than 600 mm/yr for unconfined aquifers in the San Joaquin Valley, which allows a link between the water table in unconfined aquifers and the surface water on an annual time scale (Brush et al., 2013). However, such shallow-aquifer recharge processes do not necessarily explain the replenishment of deeper, semi-confined aquifers below the Corcoran Clay and clay-lens system.

Planned or intentional replenishment of aquifers through MAR is a successful adaptation strategy that banks water for use later, for instance during droughts (Dillon, 2005; Jakeman et al., 2016; Zheng et al., 2021), thereby increasing the resilience of groundwater resources to climate change. In arid and semiarid regions, such as the lowland CV adjacent to the Sierra Nevada (Fig. 1a, Fig. 2), the availability of surplus water, such as floodwater, in addition to other factors, such as geomorphology, hydrology, soil conditions, land use, and economic conditions, determines the success of MAR (Ghasemizade et al., 2019; Kourakos et al., 2019, 2023; Marwaha et al., 2021).

However, while intentional recharge through basins, unlined canals, and injection wells can be locally effective, their ability to offset groundwater depletion across the CV, particularly in deep semi-confined aquifers, is constrained by the spatial and temporal mismatch between areas of severe groundwater overdraft and areas or periods with surplus surface-water availability

https://doi.org/10.5194/egusphere-2026-3061
Preprint. Discussion started: 11 June 2026

(Alley, 2002; Ayres et al., 2021; Escriva-Bou et al., 2021; Siebert et al., 2010; Zektser & Everett, 2004). Thus, large-scale natural recharge to deep (semi-)confined aquifers below semi-confining systems, i.e., at depths of several dozen meters, remains essential for replenishing dryland groundwater resources. In contrast to artificial recharge, the mechanisms of natural recharge to deep aquifers in the CV remain elusive.

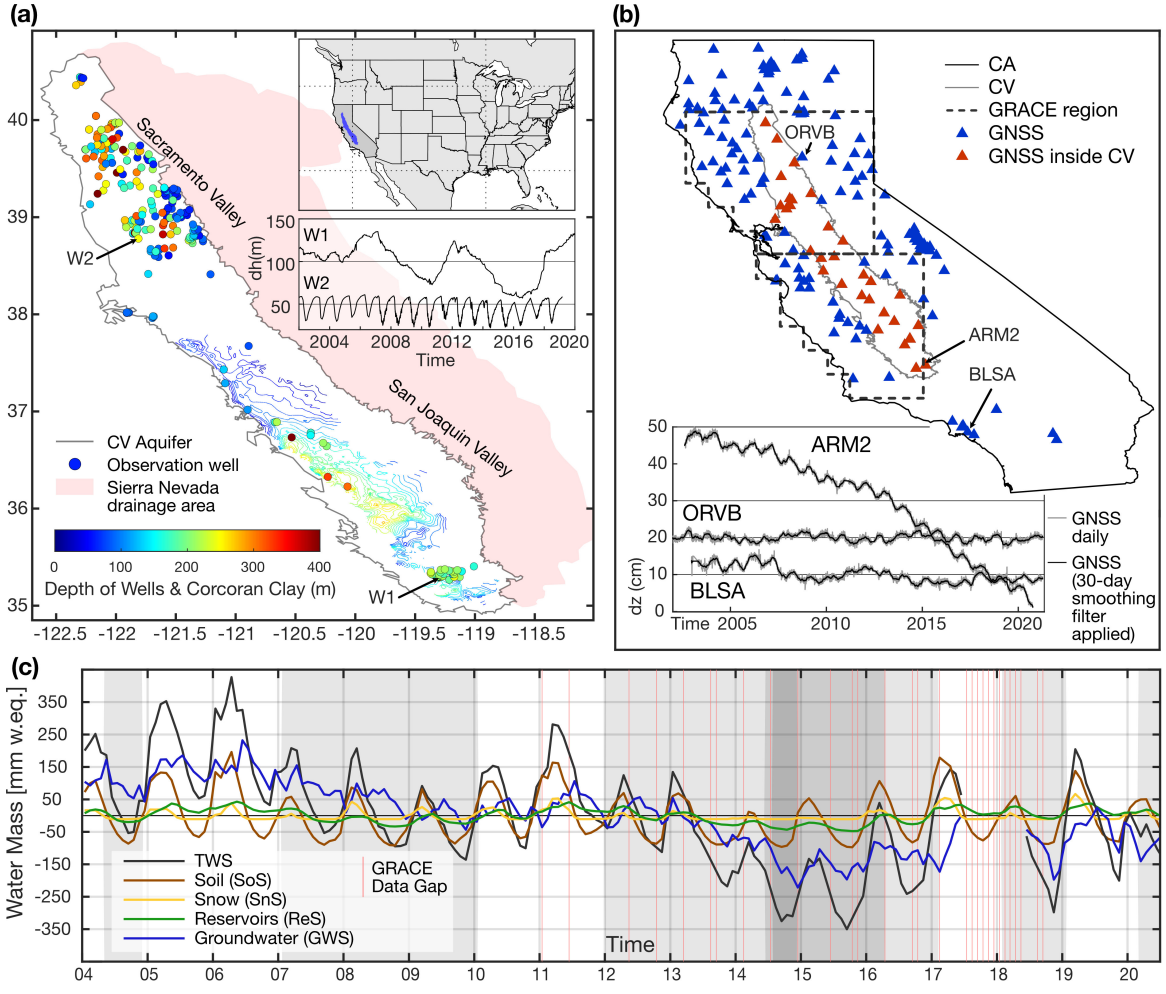

Figure 1: Overview of study area and data sets applied in this study. (a) Study area and hydrogeological datasets: Outline of the Central Valley aquifer system (grey line, A_{CV} = 53,672 km2), Sierra Nevada drainage area (red shade, A_{SN} = 63,780 km2), location and depth of observation wells that provide measurements at depth of 50 m and deeper, and lateral coverage and depth of the confining Corcoran clay layer (source USGS: https://water.usgs.gov/GIS/metadata/usgswrd/XML/pp1766_corcoran_clay_depth_feet.xml). See Figure S4e and S4f for histograms of well depths. The top inset indicates the location of the study area over the contiguous US. Bottom inset shows time series of two selected well sites, W1 (#352958N1193011W001) and W2 (#387793N1218123W004). (b) Geodetic data sets: Mass change regions of JPL GRACE mascon solutions (black dashed line) and location of GNSS sites from the University of Reno, Nevada (red and blue triangles). Red triangles mark stations located inside the Central Valley (CV), and blue triangles those outside the CV aquifer boundary. (c) Time series of TWS from GRACE, composite hydrological storages, and estimated GW storages are averaged for the GRACE region shown in panel a, after Ojha et al. [2019]. Gray shaded background areas (light, medium, dark gray) indicate that the USDM identifies >30% (>30%, >60%) of California's area to be in moderate (exceptional, exceptional) dry condition (compare Fig. S3).

https://doi.org/10.5194/egusphere-2026-3061
Preprint. Discussion started: 11 June 2026

One potential source of such natural recharge is the Sierra Nevada snowpack. California's wet and dry seasons occur during November-April and May-October, respectively, with a large portion of the Sierra Nevada's precipitation falling as snow during the winter that supplies snow melt in spring (Fig. S1, S2). The Sierra Nevada's snowpack is thought to regulate surface water availability in the CV during the summer (Faunt, 2009; Peterson et al., 2003; Urióstegui et al., 2017). Isotope studies and streamflow analyses of snow-dominated mountainous watersheds in the western USA suggest that snowpack-derived snowmelt significantly contributes to groundwater recharge, depending on the existing geology (Earman et al., 2006; Tague et al., 2008; Tague & Grant, 2009). However, the mechanisms linking the CV's deep aquifer recharge to precipitation, underground storage, and water transport in the Sierra Nevada are not well-established and disputed in the literature (Huth et al., 2004; Jódar et al., 2017; Liu et al., 2017). However, given the low water flow velocity underground, deep valley aquifers adjacent to high mountains, such as the CV, are expected to be recharged by lateral flows from higher elevations (Feth, 1964). The two main processes considered are Mountain Front Recharge (MFR) and Mountain Block Recharge (MBR, Fig. 2) (Somers & McKenzie, 2020). MFR often directly recharges shallow, unconfined aquifers and raises the water table near streambeds from the mountain front to the basin aquifer (e.g., Visser et al., 2018). MBR replenishes deeper, often confined, and semi-confined aquifers laterally connected to high mountain aquifers (Somers & McKenzie, 2020). MBR occurs through fractures in the mountain block, hydraulically connected to deep valley aquifers. Despite their proximity, there is no consensus on the role of MBR from the Sierra Nevada's granitic bedrock block into the CV aquifers; thus, it is not considered explicitly in current large-scale hydrological models used in water management assessments (Faunt, 2009; Hanson et al., 2012; Markovich et al., 2019). Meixner et al. (2016) lumped both processes into mountain system recharge (MSR) and estimated that it accounts for ~20% of total GW recharge in the CV, with the rest from diffuse and irrigation recharge in shallow layers. Recent modeling experiments indicate that MFR drives almost all the MSR to the CV aquifers (Schreiner-McGraw & Ajami, 2022). However, another study based on hydrological modeling concludes that MBR is more important and contributes up to 23% of the total GW recharge to the CV (Gilbert & Maxwell, 2017). A more recent study suggests greater hydraulic connectivity between the Sierra Nevada and CV aquifers. Based on hydrochemical and isotopic data (Armengol et al., 2024), 31-50% of sampled groundwater exhibits a chemical signature consistent with deep MBR. These hydrogeological studies generally agree on the role of MSR components. However, they disagree on the importance of MBR for recharging deep valley aquifers in the CV, and their spatial extent remains limited to smaller watersheds rather than the entire CV.

Resolving the role of MBR is essential for assessing the future resilience of the CV aquifer system under climate change. If deep valley aquifers are hydraulically connected to high-elevation mountain water storage, then changes in Sierra Nevada precipitation, snowpack accumulation, and snowmelt timing may directly affect the replenishment of deep groundwater resources in the CV. This is particularly important because drought frequency and intensity have increased globally (Fox-Kemper et al., 2021), including in California (Fig. S3), while elevation-dependent warming (Pepin et al., 2015) disproportionately affects water availability and storage in high mountains. Over the last decades, increased evapotranspiration, decreased or delayed precipitation, and snowfall have led to severe snow droughts in the western USA, including the Sierra

https://doi.org/10.5194/egusphere-2026-3061
Preprint. Discussion started: 11 June 2026

Nevada (Harpold et al., 2017; Hatchett & McEvoy, 2018; Mote et al., 2018). The low-snow years are expected to occur more regularly in the coming decades (Siirila-Woodburn et al., 2021). Ignoring the MBR contribution, if relevant, may result in overestimation of the resilience of the lowland aquifer to climate change and excess freshwater demand.

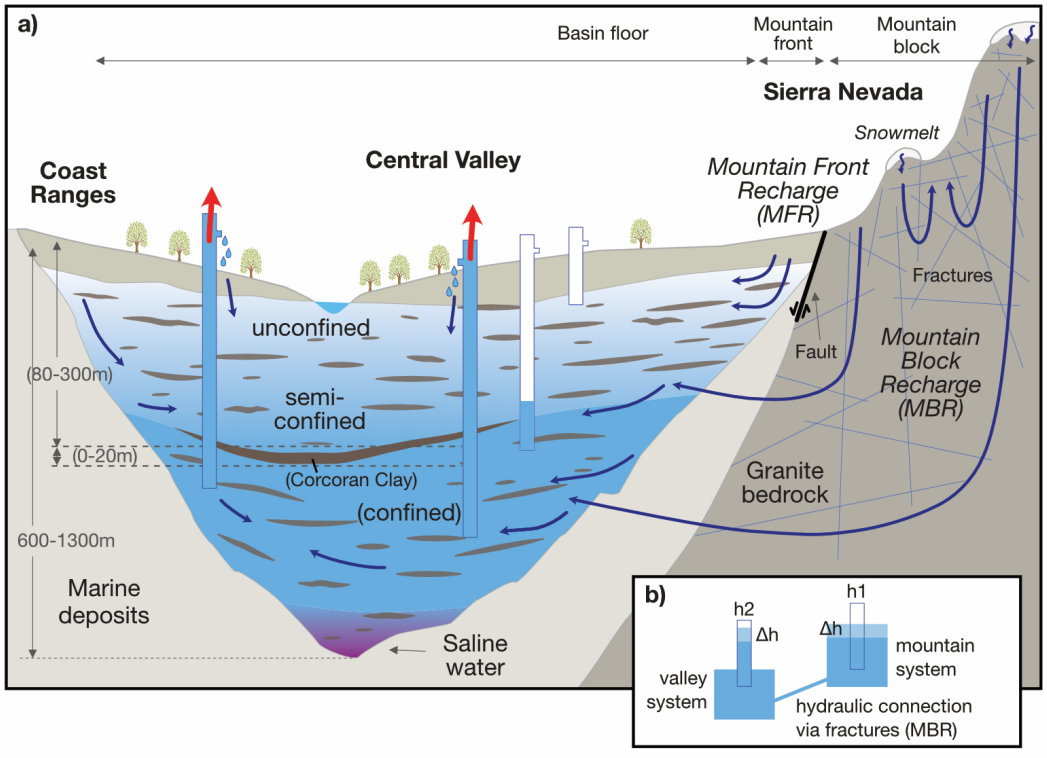

Figure 2. Conceptual and process-based sketch of pressure propagation and recharge in the Sierra Nevada to deep aquifer layers of the Central Valley. (a) Hydrogeological setting in the Central Valley (~400 m a.s.l.) and Sierra Nevada (up to ~4000 m a.s.l.). Indicated are major groundwater fluxes in and out of deep aquifer layers, including mountain front and mountain block recharge (MFR and MBR). The confining unit of the Corcoran clay is only present in the southern San Joaquin Valley, where pumping is more intense compared to the northern Sacramento Valley (Fig. 1a). This graph is inspired by Faunt et al. (2009) (Fig. A9 therein), Smith et al. (2017) (Fig. 2 therein), as well as Somers and McKenzie (2020) (Fig. 5 therein). (b) Simplified conceptual sketch focusing on the MBR system. The two aquifer systems, the valley and mountain aquifers, are hydraulically connected via fractures in the mountain block. The mountain system is elevated relative to the valley system, generating recharge from the mountains toward the valley. A change in the pressure head (h1) in the mountain system would lead to a change in the pressure head of the valley system (h2). The pressure change in the mountain propagates according to Equation 1 and in 1D simplification according to Equation S5 to depth, independent of the cross-sectional area of the conduit, and it can precede the actual flow of water volume (mass) that is dependent on the cross-sectional area of the conduit (see also Supplementary Text S2).

Remote sensing techniques provide basin-scale proxies of groundwater dynamics through complementary physical signatures: changes in the gravity field observed by the Gravity Recovery and Climate Experiment (GRACE) reflect regional total water mass variations, while surface deformation measured by Global Navigation Satellite System (GNSS) and Interferometric Synthetic Aperture Radar (InSAR) captures (semi-) confined aquifer-system response to depletion and recovery of water pressure and storage underground as well as crustal loading response to total water mass change (Bürgmann et al., 2024; Carlson et al., 2024; Jaramillo et al., 2024; White et al., 2022). Previous studies using high-resolution deformation maps suggest

https://doi.org/10.5194/egusphere-2026-3061
Preprint. Discussion started: 11 June 2026

direct recharge of deep aquifers near the mountain front following heavy precipitation events and during wet years when surface water supplies are in surplus (e.g., Neely et al. 2021). However, these studies focus on local features below alluvial fan units along the mountain foots, and not on areas with impermeable clay layers separating shallow and deep aquifers (Faunt, 2009; Shirzaei et al., 2019). There is also no evidence of vertical fractures (Carlson, Shirzaei, Ojha, et al., 2020) in the CV to provide a direct pathway for the downward flow of surface water. Argus et al. (2022) use remote sensing data and hydrological models to quantify MBR from the Sierra Nevada to the CV at about 5 km^3/yr, but neither distinguish possible contributions from MFR nor provide a conceptual model of the deep aquifer recharge mechanisms. Thus, existing remote-sensing studies indicate that geodetic observations can detect large-scale groundwater-storage dynamics, but how these observations relate to specific mechanisms linking Sierra Nevada water storage to deep aquifer recharge in the CV remains unresolved.

Existing hydrogeological and modeling studies provide important local and process-level insights, but they differ in their assessments of the importance of MBR relative to MFR, diffuse recharge, and irrigation return flow, and they rarely provide basin-scale observational evidence linking Sierra Nevada snowmelt to deep aquifer dynamics. Here, we investigate these connections using multiple observational datasets that capture complementary signatures of groundwater dynamics. Specifically, we aim to **(1)** Characterize annual groundwater dynamics across the CV–Sierra Nevada system using independent hydrologic, geodetic, and climate observations; **(2)** Identify whether a link between Sierra Nevada snowmelt and deep aquifer recharge in the CV is feasible; and **(3)** Assess whether MBR can have a detectable basin-scale signatures printed in the observed time lag among groundwater storage, groundwater levels, and deformation peaks.

We apply a robust data-driven statistical framework and wavelet-based signal decomposition schemes to investigate seasonal variations in geodetic remote sensing and hydrologic datasets across the CV and the Sierra Nevada. The data sets include groundwater level (GWL, Fig. 1a, S4), surface deformation from InSAR and GNSS (Fig. 1b, S5), GRACE satellite-derived total water storage (TWS) variations, soil water storage (SoS), snow storage (SnS) and reservoir storage (ReS, Fig. 1c). Through time-frequency and correlation analyses, we identify hidden and non-stationary patterns in time series and quantify their relationships. Lastly, we apply a first-order diffusion model to examine the feasibility of the relationships inferred by our data-driven analysis. The intellectual contribution of this study is a basin-scale, multi-sensor observational framework for evaluating whether Sierra Nevada snowmelt can contribute to deep aquifer recharge in the CV via MBR, thereby complementing local hydrogeological studies and large-scale groundwater models.

2 Data and Methods

2.1. Water Storage Components, Precipitation, and Snow Melt

GRACE and GRACE Follow-on missions (hereafter referred to as simply GRACE) monitor monthly changes in the Earth's gravity field at a spatial resolution of ~300-400 km, which are converted to equivalent TWS changes close to the surface (Schmidt et al., 2008; Tapley et al., 2004). In California, associated mass variations can be attributed to terrestrial water-cycle dynamics on sub-seasonal to interdecadal timescales. Water flow processes on and below the surface change the region's total

https://doi.org/10.5194/egusphere-2026-3061
Preprint. Discussion started: 11 June 2026

amount of water stored in the soil, snowcap, surface (including reservoirs and rivers), and groundwater. With that, GRACE total water storage variations reflect water loss, e.g., due to drought or human activities like intense groundwater pumping, as a mass deficit. Vice versa, during wetter periods, a water surplus is detected. This allows groundwater storage in large aquifers to be predicted if storage changes in all other components can be quantified and removed from GRACE TWS (Famiglietti et al., 2011; Scanlon et al., 2012).

Here, we derive changes in groundwater storage (GWS) from GRACE observations using an approach similar to that of Ojha et al. (2019). We retrieve GRACE TWS variations from the RL06 Level-3 product from NASA's Jet Propulsion Laboratory (JPL) that solves regional mass variations at a resolution of 3 degrees. JPL applies a coastal resolution filter for mascon cells at the coast that corrects for signal leakage into oceans, which is why the mascon cells we use here for the CV are cut off at the coast, as shown in Figure 1b. We do not apply JPL-mascon scale factors because we calculate groundwater changes at this native resolution and assume that leakage between the mascon tiles is negligible. A linear interpolation is applied to oversample GRACE data from their original irregular monthly sampling to a regular monthly time series before further combining them with other datasets. To separate GWS changes from GRACE TWS, we retrieve mass variations in other storage compartments from multiple data sets. We acquire soil moisture variations from all available soil layers in the NOAH, CLSM, and VIC models of the Global Land Data Assimilation System (GLDAS) Version 2.1 (Beaudoing et al., 2016; Rodell et al., 2004) at 0.25 (Noah) and 1-degree (CLSM and VIC) resolution, respectively, for the entire GRACE period. We average the three models to one ensemble dataset for further analyses after resampling them to a uniform 0.5-degree resolution (Fig. 1c). For comparison, we also retrieve soil storage changes from the WaterGAP Global Hydrological Model (WGHM, version 2.2d) at 0.5-degree resolution, which is available until 2016 (Fig. S12a). We integrate reservoir storage (ReS) changes from 18 reservoirs with capacities greater than or equal to 0.9 km^3 within the margins of the two mascon cells covering the CV (GRACE region, Fig. 1b), retrieved from the California Department of Water Resources (CDWR, 2017). Snow storage (SoS) changes are acquired in the form of snow water equivalent from the Snow Data Assimilation System (SNODAS) (NOHRSC, 2004) over the contiguous United States since the end of 2003. A recent comparison of operational and retrospective model datasets for the western United States indicates differences in the spatial distribution of snow cover relative to airborne snow-observing data (Yang et al., 2023). However, these do not significantly impact the timing of maximum SoS based on spatial averages for the Sierra Nevada Region, as we apply them here (see Fig. 7 therein). Monthly water mass variations for each storage compartment are summed across the GRACE region, and the regionally aggregated SoS, SnS, and ReS variations are removed from GRACE TWS variations after Ojha et al. (2019). The resulting time series for each storage compartment, including groundwater storage changes during both GRACE mission periods, are shown in Figure 1c. We assume the GRACE-based GWS estimate is dominated by groundwater variations in the CV, where aquifer storage capacity is likely much larger than that in the SN Mountains.

From the SNODAS dataset, we further retrieve driving and output variables related to snow cover, including 'solid'- and 'liquid precipitation', and 'snowmelt runoff at the base of the snowpack', to investigate these fluxes in the Sierra Nevada (Fig.

https://doi.org/10.5194/egusphere-2026-3061
Preprint. Discussion started: 11 June 2026

S1, S2) and their correlation to groundwater dynamics. For that, we correct liquid precipitation for canopy interception by a relative value of 20%, adapting this estimate from previous studies for mixed forests in the Sierra Nevada (Bales et al., 2011).

2.2. Groundwater Levels

Groundwater availability in the CV is conventionally monitored using water-level changes in observation and irrigation wells. The data archives from the United States Geological Survey (USGS) and the California Department of Water Resources (CDWR) provide more than 40,000 records from wells within the CV. The records have varying start dates, not all are continuously monitored to today, and only some provide sufficient temporal sampling to study seasonal variations in GWLs. For this study, we have screened 'daily data' and 'field data' archives from the USGS (USGS, 2021) as well as 'continuous data' and 'periodic data' archives from CDWR (CDWR, 2019a) in California and selected records that cover the GRACE mission period from 2002 to 2020. We have excluded records labeled as 'irrigation well' and only selected sites labeled 'observation well'. This significantly reduces the number of data points, especially in the south. However, water levels in observation wells are less likely to be affected by the localized reduction in pressure during and after pumping from the well, which is an important criterion. Levels in observation wells are more likely to reflect regional changes in pressure and storage across the entire aquifer. Further selection criteria for observation wells include distance from known pumping centers and historical stability of water levels. While it is challenging to find wells entirely unaffected by pumping, our methodology aimed to minimize this impact.

In addition, we categorized data entries more than 3.5 times the standard deviation of the detrended time series as outliers and excluded them. Moreover, about half of the records have daily sampling rates, and we excluded entire records from the field/periodic datasets, which had fewer than six entries per year on average. From the initial dataset, 2128 time series (371 from USGS and 1727 from CDWR) provide observation records from 2002 to 2020 inside the CV. Only 682 records cover at least three years with less than 3 months of gap (Fig. S4). We remove well measurements taken at depths shallower than 50 m to exclude the bulk of wells that likely tap unconfined layers and are located above clay lenses distributed throughout the CV aquifer, thereby creating (semi-)confined conditions. We inspected top-to-bottom perforation depths from CDWR and aquifer codes from USGS to classify wells representative of deeper aquifer zones (see Fig. S4). While long screen intervals can lead to mixed shallow and deep aquifer signals, this selection provides the best available separation based on the existing metadata. We are left with 457 records collected at depths greater than 50 m, allowing us to focus on measurements from semi-confined and confined aquifers. About half of these records are longer than 10 years (Fig. S4a-c), and their average depth is 155 m. We note that these records were collected at only 250 unique well locations (circles in Fig. 1a), with some sites containing up to five nested-level meters (Fig. S4d). Most of the lowest sensors at each site are located 50 m to 300 m below the surface, with about half of the sensors reaching no more than 200 m, and only a few are 450 m or deeper (Fig. 1a, S4e, f). The average depth of the lowest sensor at unique well locations is 180 m. Most usable wells are in the northern Sacramento Valley, and only two dozen sites are in the southern San Joaquin Valley, where only 22 wells measure water level variations at depths below the

https://doi.org/10.5194/egusphere-2026-3061
Preprint. Discussion started: 11 June 2026

Corcoran clay, and most of them fall into the eastern slope of the basin, between the Sierra Nevada and the deepest point of the Corcoran Clay and Valley. Examples of GWL time series are shown in Figure 1a.

2.3. Surface Deformation

Surface deformation due to TWS change, including GWS, occurs through two different processes. Total water mass deforms Earth's elastic crust, resulting in subsidence for an increase in water mass and uplift for a decrease in water mass. This deformation process has been described and inverted to quantify TWS in California (Adusumilli et al., 2019; Argus et al., 2022; Borsa et al., 2014; Carlson et al., 2022; Carlson, Shirzaei, Werth, et al., 2020; White et al., 2022). A second poroelastic deformation process occurs only in semi-confined or confined aquifers, where pore spaces and the rock's granular matrix compact, and groundwater levels fall under reduced water pressure. The opposite happens for increasing water pressure. The poroelastic deformation of unconfined aquifers is negligible due to relatively small values of the Biot-Willis coefficient linking fluid pressure to solid matrix confining stress (Wang, 2000), which we demonstrated in Supplementary Text S1. Changes in water pressure in a confined aquifer can either be caused by net recharge or discharge, i.e., GWS change, in the aquifer itself, or initiated by water pressure propagating between the aquifer and a hydraulically connected outside region (Fetter & Kreamer, 2022). Decades of declining groundwater levels in the CV deep aquifers have caused continuous land subsidence at the surface, with the effects most severe during droughts (Galloway et al., 1999; Ojha et al., 2018; Smith et al., 2017; Vasco et al., 2022). It has been shown that elastic loading deformation in California is of the opposite sign and up to two magnitudes smaller than the poroelastic deformation occurring at the surface of the CV (Carlson, Shirzaei, Werth, et al., 2020).

To study seasonal variations in vertical land motion (VLM) since the early 2000s, we use vertical deformation time series from the daily tenv3 GNSS solutions from the Nevada Geodetic Laboratory (NGL). The solutions are processed at NGL using GipsyX software and are transformed into the IGS14 reference frame. Additional processing information is available on the NGL website (http://geodesy.unr.edu/gps/ngl.acn.txt). We do not apply any further corrections to the GNSS time series for the rest of our analysis. From 1184 stations in California, we selected 170 with at least 5 years of record between 2002 and 2020 and exhibiting a seasonal amplitude greater than the time series median standard deviation. This selection criterion discards stations with near-zero seasonal amplitude and those with observations dominated by noise, mainly located outside confined aquifer areas. Most selected stations began observations around 2008 and continued for 15 years (Fig. S5b). Of these stations, 37 are located within the CV boundaries (red triangles, Fig. 1b). Example time series at three sites throughout the study area are shown in the inset of Figure 1b. Using a time-frequency analysis, we determine the seasonal component of GNSS vertical land motion and the timing of maximum uplift and subsidence (see Section 2.4).

We further measure surface deformation along the line of sight (LOS) over the southern CV using InSAR. The SAR dataset includes 238 C-band images from the descending track, path 144, of the Sentinel-1A/B satellites, spanning 2015/11/27-2022/12/20. We apply multi-looking factors of 32 and 6 in range and azimuth to obtain a pixel dimension of ~75m by ~75m. We use GAMMA software (Werner et al., 2000) to create a large set of interferograms. The interferograms are selected so they form triplets, and the numbers of short, medium, and long temporal baseline pairs are comparable to minimize the phase

https://doi.org/10.5194/egusphere-2026-3061
Preprint. Discussion started: 11 June 2026

closure error impact (Lee & Shirzaei, 2023). We apply the wavelet-based InSAR (WabInSAR) algorithm (Lee & Shirzaei, 2023; Shirzaei, 2013; Shirzaei et al., 2017) to perform a multitemporal interferometric analysis of the SAR dataset and create high-accuracy maps of surface deformation time series. A Shuttle Radar Topography Mission (SRTM) Digital Elevation Model (DEM) of 1-arcsecond (~30 m) spatial resolution (Farr et al., 2007) and precise satellite orbital information are used to estimate and remove the effect of topographic phase and flat earth correction (Franceschetti & Lanari, 1999). The absolute phase values are obtained by applying a 2D minimum-cost flow algorithm (Costantini, 1998), then combined to create a Line-of-Sight (LOS) time series of surface deformation using a reweighted least-squares approach. The spatially correlated and temporally uncorrelated atmospheric delay are also estimated and removed (Shirzaei, 2013).

2.4. Time-Frequency Analysis

To investigate temporal variations in water storage components, GWLs, and deformation data, we perform a time-frequency analysis using a continuous wavelet transform, following the approach of Shirzaei et al. (2013). The wavelet transform allows signals to be decomposed into building blocks based on their frequency content. In contrast to the Fourier transform, wavelets can handle non-stationary signals and localize signal energy in both the time and frequency domains (Goswami & Chan, 1999). Wavelets have a key parameter scale (or dilation), which stretches or squishes the wavelet function and relates to the analyzed signal frequency. To perform wavelet analysis, we use the MATLAB packages provided by Torrence and Compo (1998) and Erickson (2019) and apply the wavelet family of derivatives of Gaussian (DOG, Fig. S6) at 200 levels of decomposition or scales. The temporal sampling of all time series is either daily or resampled at daily intervals using linear interpolation.

Figures 3 and S7 illustrate our approach with an example of groundwater level time series at the DWR well #387793N1218123W004 (Fig. S7a). The wavelet power spectrum map (PSM, Fig. 3a and S7b) shows the signal's energy breakdown into several frequency components and their relative importance, as indicated by the PSM amplitude. A cone-of-influence overprinted on the spectrum indicates areas where edge effects play a role, and therefore, the PSM cannot be interpreted. Signal energy in areas within the cone of influence is strongest at periods of about one year, with contour lines indicating their statistical significance relative to white and red noise (with a lag-1 autocorrelation parameter of 0.85 for the latter) (Torrence & Compo, 1998). Figure 3 also shows examples of wavelet PSM for selected GWL, VLM, and TWS component time series.

To isolate the annual component from the time series, we set the PSM to zero except for periods between 0.75-1.25 years and then apply an inverse wavelet transform of the new PSM (Fig. S7c). This approach considers that the annual components in climate-related processes do not have an exact one-year period. We further analyze the reconstructed annual signals to characterize the timing of annual maxima, minima, and the timing of fastest rate declines and increases (blue, red, and gray circles in Fig. S7c). We summarize the annual values for several years through temporal averaging using the median operator to retrieve the timing of maximum in the annual signal (e.g., as shown in Fig. 4). We successfully apply this method to time series of original daily to monthly temporal sampling resolution, after oversampling all datasets for a regular daily time series

https://doi.org/10.5194/egusphere-2026-3061
Preprint. Discussion started: 11 June 2026

using linear interpolation (see example for original monthly time series from well #387626N1213651W002 in Fig. S7d-f). The same approach is applied to the time series of GWL, TWS components, GNSS and InSAR vertical deformation.

Probability density functions (PDFs) for the spatiotemporal variation of timing of annual peaks were calculated using MATLAB's probability density estimator *kdensity()*, based on a normal kernel function for univariate distributions, and apply a kernel smoothing window with an optimized bandwidth for normal densities. Since sample sizes are much larger than the minimum of ~30 suggested by the central limit theorem (Meyer, 1970), the outcome of the statistical analysis is independent of the assumed distribution (e.g., normal) of the individual samples. Thus, choosing a normal kernel function has no impact on the results.

2.5. First-order Assessment of Pressure Propagation from Mountains to Deep Aquifers

To evaluate whether the observed temporal lag between mountain water availability and groundwater level variations in the CV is physically plausible, we conduct a simplified first-order analysis of vertical pressure propagation through the mountain block. This analysis is not intended to represent the full hydrogeologic complexity of the system, but rather to assess whether the magnitude of the observed delays is consistent with reasonable ranges of hydraulic properties reported for fractured bedrock environments (Saar & Manga, 2003; Somers & McKenzie, 2020; Talwani & Acree, 1985; Wang, 2000).

In the Sierra Nevada, a substantial fraction of snowmelt and precipitation infiltrates into fractured crystalline bedrock (Fig. S1, S2), increasing pore-fluid pressure in shallow mountain aquifers (Bales et al., 2011; Uriόstegui et al., 2017). These aquifers are hypothesized to be hydraulically connected to deeper aquifer systems in the CV through MBR pathways (Faunt, 2009; Somers & McKenzie, 2020), see also Fig. 2a. The mountain block fractures provide hydraulic connectivity between elevated mountain aquifers and the valley system, as further highlighted by a simplified sketch in Figure 2b. Hence, a change in the pressure head (h_{p1}) in the mountain system would lead to a change in the pressure head of the valley system (h_{p2}). Under this conceptual framework, temporal variations in pore pressure may propagate through the connected system prior to significant groundwater mass transport (Supplementary Text S2) (Fetter & Kreamer, 2022; Viswanathan et al., 2022).

We approximate this process using a one-dimensional vertical diffusion formulation for pore-fluid pressure propagation:

$$\frac{dP}{dt} = \kappa \cdot \nabla^2 P \,, \tag{1}$$

where hydraulic diffusivity, κ, governs the rate of pressure, P, transmission. We consider a range of diffusivity values representative of fractured bedrock systems reported in the literature (Saar & Manga, 2003; Gao et al., 2000; Montgomery-Brown et al., 2019) and evaluate the time required for a seasonal pressure signal to propagate from shallow mountain aquifers to depths corresponding to confined aquifers in the CV. The model has recently been successfully applied to assess groundwater-surface water connectivity surrounding Lake Mead (Khorrami et al., 2025). Further details are provided in Supplementary Text S3.

This simplified approach assumes saturated conditions and does not explicitly account for vadose-zone processes, fracture-network heterogeneity, or complex three-dimensional flow paths. In addition, fractured mountain aquifers may exhibit

https://doi.org/10.5194/egusphere-2026-3061
Preprint. Discussion started: 11 June 2026

complex storage behavior due to secondary porosity and locally unconfined conditions, which can alter the relationship among hydraulic-head changes, pressure propagation, and groundwater flow. As such, the approach should be viewed as a feasibility assessment rather than a predictive representation of the system, providing only a first-order estimate of whether the observed phase lag between snowmelt and groundwater-level response is consistent with plausible pressure-propagation timescales.

3. Results

3.1 Year-to-Year Water Variability

The time series of TWS variations obtained from the GRACE satellites (Tapley et al., 2004, 2019) and their components measured through in-situ observations (e.g., wells) (Alam et al., 2021) or water balance models (Faunt, 2009; Li et al., 2018) are characterized by annual variations attributed to overall dynamics in the terrestrial water cycle (Tang & Oki, 2016). Several example time series are shown in Figure 1c. A less obvious pattern comprises the interannual variations in the amplitude of the annual signal. Identifying the amplitude and timing of the peak annual and interannual signal components allows for resolving the temporal scale at which the connected systems interact.

To this end, we apply wavelet-based time-frequency analysis to extract hidden patterns in the datasets (see Section 2.2.1 and Fig. S6). The results of the time-frequency analysis are shown as a PSM, which distributes the signal's power across frequencies (or periods) and time intervals (Fig. 3, S7). We find that maximum amplitudes characterize the PSMs associated with different time series at equivalent periods of 1 year and 3-8 years (Fig. 3). These frequency components are associated with general variations in water availability associated with atmosphere-ocean interactions, influencing water cycles in the Southwest USA (Quiring & Goodrich, 2008). Significant drought periods, such as during 2007-2009 and 2012-2015 (Fig. S3), correspond with cool phases of El Niño Southern Oscillation (ENSO) recurring every 3-7 years, the cool phase of the Pacific Decadal Oscillation (PDO), and the warm phase of the Atlantic Multidecadal Oscillation (AMO) (McCabe et al., 2004; Quiring & Goodrich, 2008). The length of our observation does not allow us to resolve signal components over a decade or longer, as indicated by the cone of influence, the shaded region in the PSM.

Some PSMs also show unique patterns. For instance, the PSMs of GWL changes (Fig. 3a) and GNSS VLM (Fig. 3b) exhibit components at periods of 0.5 and 3 years, although the 0.5-year component for VLM disappears after 2008. In contrast, the PSM of SnS (Fig. 3e) shows only a transient component over 3 years. PSM of GWS variations (Fig. 3g) shows a transient component of a 1-year period. Notably, the location and amplitude of peak PSM vary over time, especially for TWS, SnS, ReS, and GWS variations, and to a lesser extent for SoS, due to changes in water availability across wet and dry seasons and between them, as well as human interventions. For instance, the amplitude of annual components was reduced or diminished during the drought years 2007-2010 and 2012-2015. During these periods, reservoirs were not refilled, and the Sierra Nevada received little precipitation, reducing the amplitude of the corresponding annual components (Fig. 3e and 3f). The amplitude of the annual component of GWS variations vanishes during the same years (Fig. 3g).

https://doi.org/10.5194/egusphere-2026-3061
Preprint. Discussion started: 11 June 2026

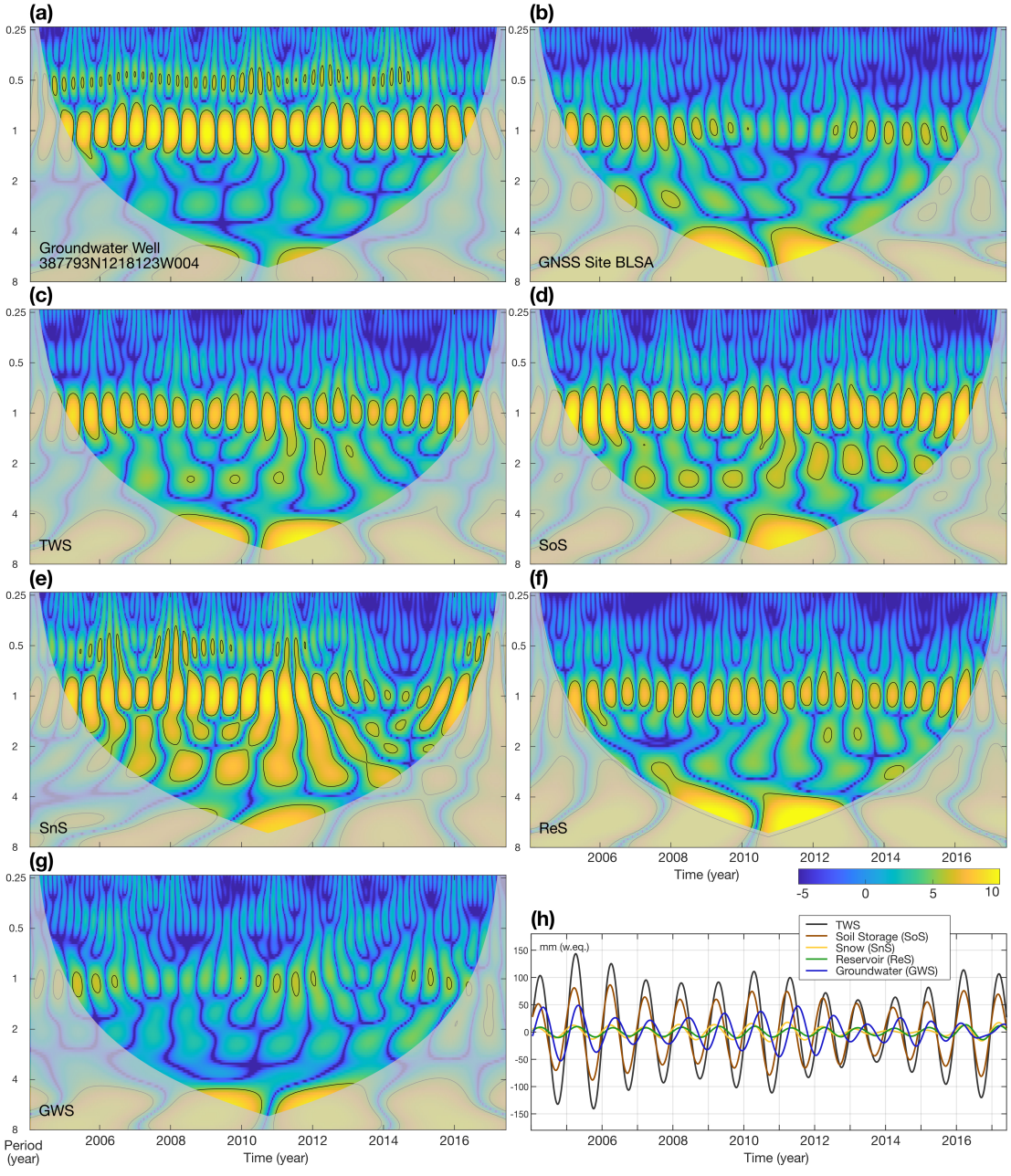

Figure 3. Wavelet time-frequency analysis. Wavelet analysis was performed on the time series from all available datasets to isolate the annual signal component. Wavelet spectrum of time series of (a) groundwater level at well 387793N1218123W004 and (b) vertical land motion at GNSS site BLSA (see Fig. 1 for their location), and of average water storage variations in the GRACE region: (c) total water storage (TWS) from GRACE, (d) soil storage (SoS) from GLDAS and WGHM, (e) snow storage (SnS) from SNODAS, (f) reservoir storage (ReS) from CDWR and (g) groundwater storage (GWS) in CV. (h) Reconstructed annual signal component for periods within the range of 0.75-0.25 years from water storage wavelet spectra shown in panels c-g.

https://doi.org/10.5194/egusphere-2026-3061
Preprint. Discussion started: 11 June 2026

Figure 3h presents the isolated annual components for all time series comprising PSM components with 0.75 to 1.25 yr periods, which exhibit nonstationary behavior, i.e., amplitude changes over time. We find that year-to-year TWS exhibits the most pronounced changes, while GWS exhibits the least. We also note that year-to-year peak extremes do not co-occur for different time series. For instance, during the 2012-2015 drought, TWS, SoS, and ReS variations exhibited their lowest amplitudes in 2013 and 2014, whereas that of GWS occurred two years later, in 2016, following the snow-poor years in 2014 and 2015. Characterizing such inter-annual variability in water cycle components improves understanding of the region's hydroclimate extremes and water storage capacity (Yin & Roderick, 2020).

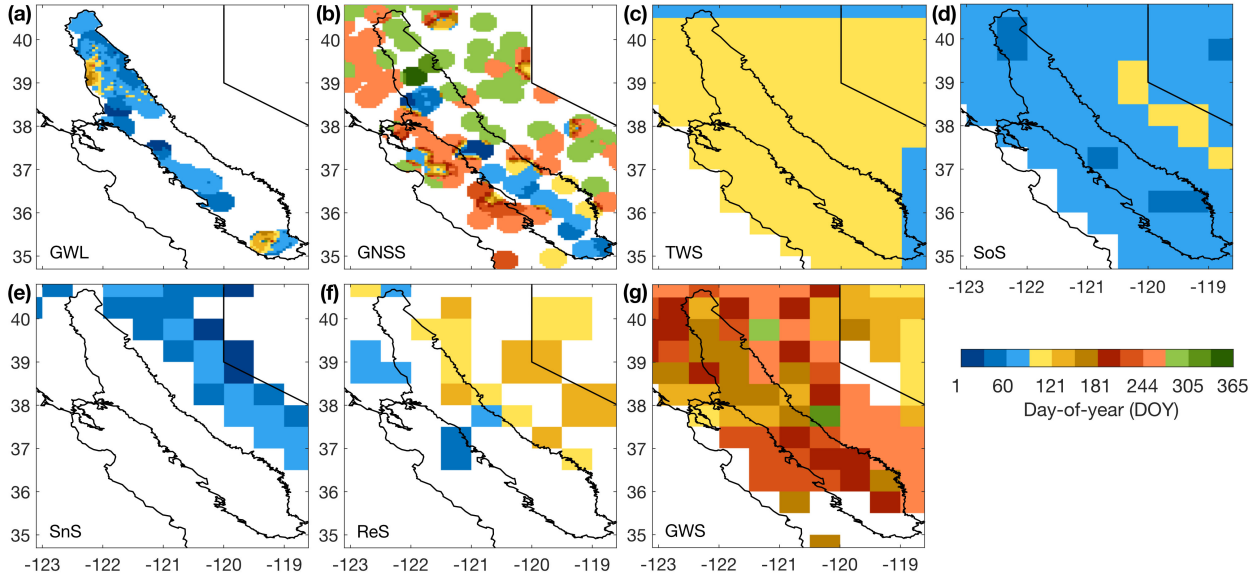

Figure 4. Timing of the annual maximum of groundwater-related signals. Timings are given in day-of-year (DOY). (a) Groundwater levels (GWL) at 250 observation sites throughout the Central Valley are provided for at least three years of data from 2002 to 2020 at depths below 50 m. (b) Vertical land motion (maximum uplift) at 170 GNSS sites throughout California with a seasonal amplitude larger than the median of the time series error standard deviation. Timing for groundwater and GNSS were inversely interpolated using a 25 km correlation radius. Remaining panels show timing of annual maximum water storage at 0.5-degree sampling resolution: (c) total water storage (TWS) from GRACE, (d) soil storage (SoS) from GLDAS-Noah, (e) snow storage (SnS) from SNODAS, (f) reservoir storage (ReS) from CDWR, and (g) resulting groundwater storage (GWS). White areas have either no data or an annual variation amplitude near zero. Annual oscillations of vertical land motion inside the CV are temporally aligned with those of groundwater level variations. In contrast, oscillations of vertical land motion outside the Central Valley are in resonance with annual oscillations of total water storage changes detected by GRACE (compare panel b with c, and Fig. 6), because maximum VLM outside the Valley is driven by minimum elastic load of the water masses. Individual values for groundwater well and GNSS sites, timing of minima, related histograms, and standard deviations of annual timing during observation periods are shown in Figures S8, S9, S10, and S11.

3.2. Timing of the Seasonal Signal

We further investigate the spatial variability of the timing of the peak annual amplitude of TWS and its components across the study region (Fig. 4). Note that spatial detail cannot be resolved from the GRACE TWS with 300-400 km spatial resolution. To this end, we identify the day-of-year (DOY) corresponding to the peak of the annual component time series, and then obtain

https://doi.org/10.5194/egusphere-2026-3061
Preprint. Discussion started: 11 June 2026

the median DOY for each time series. Figure 4 plots the median peak DOY for each dataset at their original spatial resolution, except for GWL and VLM, where the values are interpolated with an inverse distance weighting scheme with a 25 km radius. The median peak DOY for GWL is uniform across the Valley (Fig. 4a, S8) with negligible interannual variability (Fig. S9). GWL peaks occur from February to March (Fig. 4a, S8a) and minima in August (Fig. S8b). The fastest GWL rate increase (i.e., the mid-point between annual minima and maxima) occurs during November (Fig. S8c), and the fastest GWL rate decrease (i.e., the mid-point between annual maxima and minima) occurs during May (Fig. S8d). These observations are consistent with the timing of the CV's maximum pumping, from April to June. A linear correlation of 0.3 was found between observation well depth and peak DOY, indicating GWL rises slightly later in the year at deeper wells (Fig. S8a, left inset). Compared with GWL, the median peak DOY of GNSS VLM in the CV is spatially more variable (Fig. 4b and S10), with negligible interannual variability (Fig. S11). We find a bimodal distribution for this peak DOY (inset in Fig. S10a), with about a third of the stations within the CV peaking from March to April and most of the remaining stations from September to October. A bimodal behavior is also observed in the median DOY of annual VLM minima. The median DOY of the fastest VLM rate increases and decreases are also obtained (Fig. S10), indicating a smaller interannual variability than that of peak DOY (Fig. S11). We further estimate the median peak DOY of TWS, SoS, SnS, ReS, and GWS within the GRACE region (Fig. 1b), all of which show spatially uniform patterns but are distinct from each other (Fig. 4c-g), with spatial DOY averages of 93, 70, 65,102, and 156 days, respectively.

We performed a similar analysis using InSAR LOS deformation observations. Figure 5a shows the LOS velocity field measuring up to 18.5 cm/yr subsidence in some parts of the San Joaquin Valley. We obtained seasonal phase (peak DOY) and amplitude (Fig. 5b, c) for the southern CV covered by the Sentinel-1 frame. These maps, together with example time series, and more clearly if detrended, indicate the presence of a clear seasonal signal (Fig. 5d). The spatial distribution of annual median peak DOY generally agrees with that of GNSS (Fig. 4b). The denser spatial sampling from the InSAR analysis, however, reveals a more detailed pattern for the propagation of the deformation. With some exceptions, we find a main feature indicating an outward propagation of the median annual peak DOY from the center of the San Joaquin Valley, especially in areas where the Corcoran clay sits deeper (compare Fig. 1a), towards the sides of the valley where the Corcoran clay sits shallower. Although it varies annually, the overall outward-propagating pattern of peak DOY remains similar across wet and dry years (Fig. S14), while amplitudes are lower in drier years (e.g., 2018, Fig. S15). We note that this result appears to contradict what Neely et al. (2021, 2024) found, who suggested an MFR-driven inward propagation of the annual peak toward the center. We address this further in the discussion section below. Figures 5c and S15 show the median and yearly seasonal amplitude of surface LOS deformation, reaching up to 4 cm, with the largest value during dry years.

Next, we investigate the empirical probability density function (PDF) of annual peak DOY associated with all components of TWS and deformation and several other relevant hydrological datasets (Fig. 6). Shown are normalized PDFs of annual peak DOY obtained for each year and each time series without temporal averaging, thus the interannual variabilities are preserved. Comparing different PDFs, we find for the Sierra Nevada that precipitation generally peaks in early January, with a mean DOY of 16 (Fig. 6a), meltwater in late February, DOY 55 (Fig. 6c), and the total water availability (combination of

https://doi.org/10.5194/egusphere-2026-3061
Preprint. Discussion started: 11 June 2026

precipitation, meltwater, and canopy interception) in late January, DOY 22 (Fig. 6b). We obtain a wide distribution for the influxes, and years with a later maximum melt typically have a larger peak, causing the right-skewed distribution of annual peak DOY of snowmelt (Fig. S2b). The annual SoS peak for the CV occurs in March, DOY 70 (Fig. 6d), ~2-3 months after precipitation peaks. SnS peaks in March, ReS and TWS ~1 month later in April, while GWS of the CV peaks in June (Fig. 6e-g). The VLM minima (i.e., subsidence) across California, outside of the CV, co-occur with TWS maxima around April, DOY 93 (Fig. 6i). In contrast, GNSS VLM inside the CV (Fig. 6j) peaks together with GWL (Fig. 6k) around March, DOY 65, and ~3 months before GWS based on GRACE and composite hydrology (Fig. 6g). Peak VLM inside the CV derived from high-resolution InSAR maps (Fig. 6k, dashed line) have a more complex distribution, with the first peak co-occurring with GNSS and well levels around the beginning of March and a later peak ranging from beginning to end of April. We further observe a 43-day delay between the total water available for recharge in the Sierra Nevada Drainage area (DOY 22, Fig. 6b) and the GWL in the CV (DOY 65, Fig. 6k).

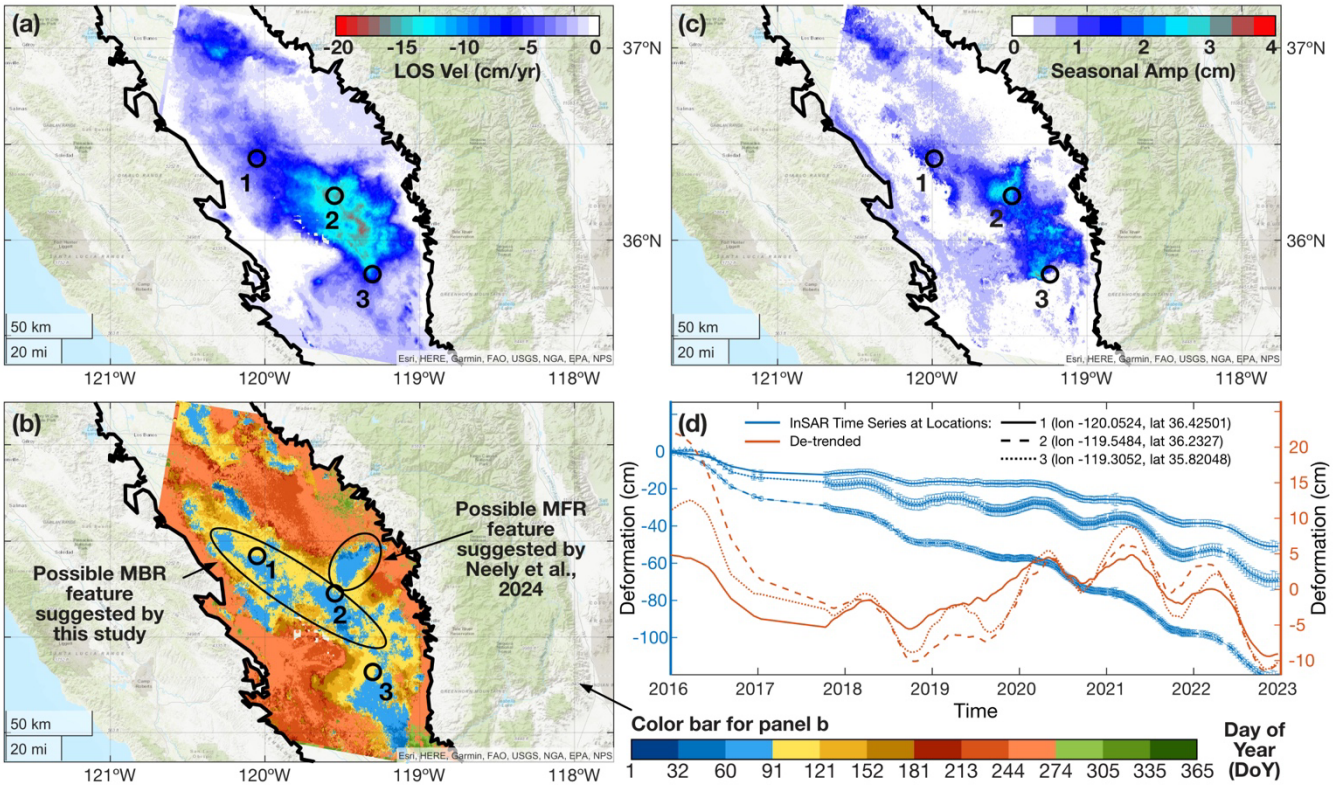

Figure 5. a) LOS velocity map for the period 2015/11/27-2022/12/20. b) Median seasonal phase (peak DOY) highlighting suggested features caused by Mountain Block Recharge (MBR) and Mountain Front Recharge (MFR), and (c) amplitude of InSAR deformation time series for water years 2016-2022. See Figs. S14 and S15 for yearly phase and amplitude maps, respectively. d) Example time series for three pixel locations marked in panel a-d. Blue graphs, scaled by the left y-axis, show the original time series with standard deviations as error bars, and red graphs, scaled by the right y-axis, indicate detrended time series at the same locations.

https://doi.org/10.5194/egusphere-2026-3061
Preprint. Discussion started: 11 June 2026

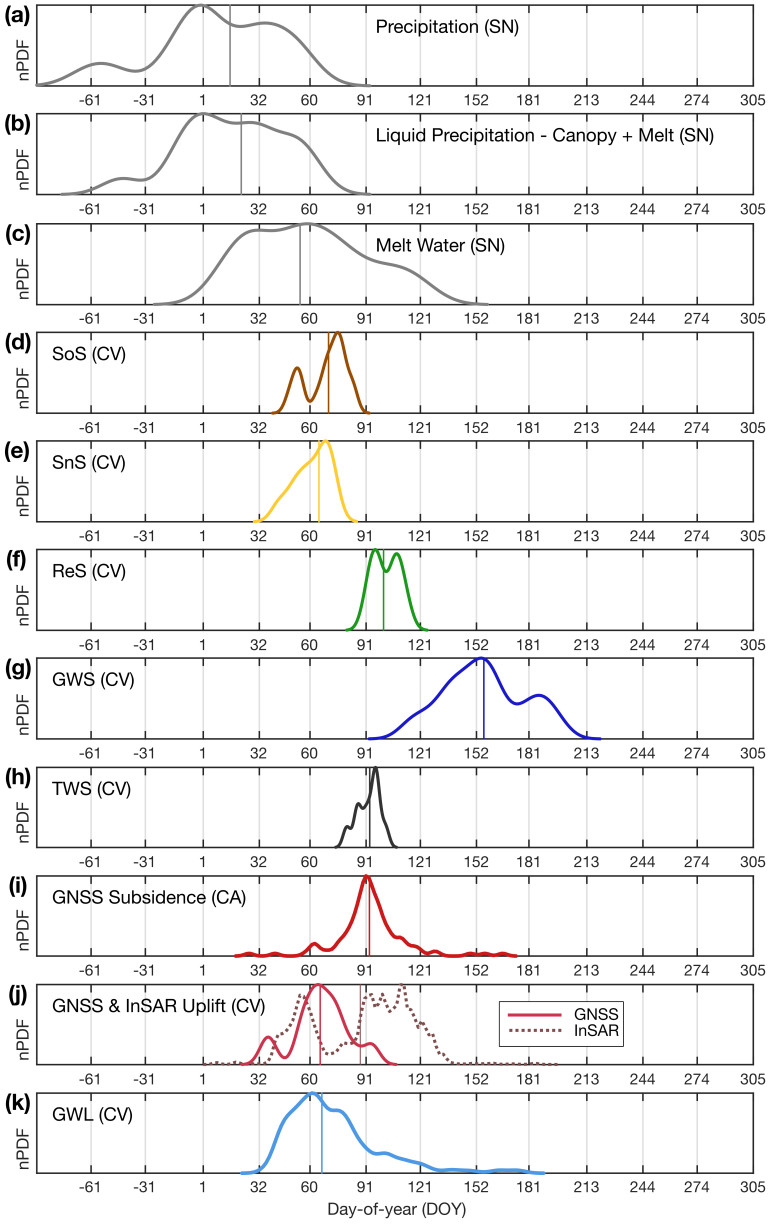

Figure 6. Normalized probability density functions for timing of annual extremes in groundwater-related signals across California. Row and line color indicate signal type: (a) total precipitation in the recharge area of the Sierra Nevada (SN, see Fig. 1a) from SNODAS, (b) Sum of liquid precipitation and melt water corrected for canopy interception in SN from SNODAS, (c) Melt water in SN from SNODAS, (d) soil storage from hydrological models for GRACE region corresponding with the Central Valley (CV, Fig. 1b), (e) snow storage from SNODAS for CV, (f) surface reservoir storage from CDWR for CV, (g) GRACE-based estimate of groundwater storage for CV, (H) total water storage from GRACE for CV, (i) vertical land motion from GNSS for all available sites in California (CA), and (j) for GNSS sites (red) in the CV only, and for InSAR pixels in the southern CV from Fig. 5 with a seasonal amplitude larger than 3 mm, and lastly, (k) groundwater levels from observation wells in CV. See Figure 1 for the location of subregions. Each function indicates the maximum probability for the timing of the annual maximum (a-i, k) or minimum (j) amplitude of the annual signal based on wavelet analysis (Fig. 3 and Fig. S7). Vertical lines represent the mean value for the timing of the annual maximum. Distribution is normalized to the maximum probability density value and results from year-to-year variation in the regionally averaged gridded datasets (a-h) and from spatial variation in well and GNSS datasets (i-k).

https://doi.org/10.5194/egusphere-2026-3061
Preprint. Discussion started: 11 June 2026

To investigate whether the mean values of the PDFs in Figure 6 differed significantly, we performed a two-sample mean-difference hypothesis test using the t-distribution (Meyer, 1970). We formulated the null hypothesis that the mean values were equal and tested it at the 0.05 significance level. The test was rejected; hence, the mean values are statistically different for all pairs of PDFs in Figure 6, except between GNSS uplift (CV) and GWL (CV), between TWS and GNSS Subsidence (CA), between SnS (Sierra Nevada) and GNSS uplift (CV), and between SnS (Sierra Nevada) and GWL (CV).

When estimating PDFs for the timing of annual peaks in SoS and GWS (Fig. 6e and 6g), variability among the individual SoS models was accounted for (Fig. S12). SoS timing varies by about ~2 months from January to February (Fig. S12c). We propagate the variation of SoS timing toward that of GWS by estimating GWS for each individual soil model (Fig. S13a). The resulting annual GWS timing varies ~2 months from May to July (Fig. S13b,c). This variability was included when calculating mean, median, standard deviation, and PDFs of annual GWS timing (Fig. 6g). Although GWS also depends on the timing of TWS, SnS, and ReS, annual amplitudes of SnS and ReS are only 10% of TWS (Fig. 1c). Therefore, they will only marginally impact the calculation of annual timing of GWS. We assume a minimal measurement uncertainty for the timing of TWS.

3.3. Feasibility of the Pressure Diffusion from the High Mountains to Deep Valley Aquifers

Assuming an existing hydraulic connection between the deep CV and the High Sierra Nevada mountain aquifers through the fractures in the mountain block, as conceptualized in Figure 2, it takes some time for the water pressure to reach depth. We provide a first-order estimate for the diffusion time, the time it takes for a seasonal pressure front to vertically diffuse from the top aquifer layers in the Sierra Nevada down to elevations of the deep CV aquifers (Section 2.5, and Eq. S5). If we quantify that using a hydraulic diffusivity $\kappa = 0.3$ m^2/s for the Sierra's crystalline fractured rocks, it takes 18-36 days for the pressure to travel vertically to depths of 600-2000 m, corresponding to the vertical distance from the high mountains to the deep aquifer layers below the Corcoran clay. Delay times for all depths at 100m increments are visualized in Figure S16, and example numerical values are provided in the inset table. We further consider a range of vertical hydraulic conductivities and evaluate diffusion times for $\kappa = 0.1$ m^2/s and $\kappa = 0.5$ m^2/s to a depth of 600-1300 m, corresponding to 34-73 days and 12-23 days, respectively (Fig. S17).

4 Discussion and Conclusions

4.1 Multi-Sensor Characterization of Seasonal Groundwater Dynamics in the Central Valley–Sierra Nevada System

Our integrated analysis reveals a coherent, cascading sequence of annual peak timing across independent hydrologic and geodetic datasets, providing a consistent system-scale picture of how pore fluid diffuses through the Sierra Nevada–CV system on seasonal timescales. Among the storage components, annual peaks progress from soil moisture and snow storage in late winter, through surface reservoir storage in spring, and finally to GRACE-derived groundwater storage in early summer (Figs. 4d–g and 6d–g). The TWS peak integrates these contributions and serves as an intermediate reference (Fig. 4c, 6h). The observation that peak GWL in deep CV aquifers occurs approximately one month after peak water availability from Sierra

https://doi.org/10.5194/egusphere-2026-3061
Preprint. Discussion started: 11 June 2026

Nevada snowmelt and rainfall combined (Fig. 6b, k) is consistent with a near-real-time hydraulic response of the deep aquifer system to mountain hydrologic forcing. Similar lag times have been documented in other mountainous regions with fractured bedrock aquifers (Meles et al., 2024; Wilson & Guan, 2004).

Independent geodetic observations reinforce this sequence. Inside the CV, where confining layers are thick and annual deformation amplitudes are large, the seasonal deformation signal from both GNSS and InSAR co-occurs with GWL variations (Figs. 4a, 4b, 5c, and 6j, 6k), consistent with poroelastic aquifer deformation driven by groundwater pressure and pumping stresses (Ojha et al., 2018; Smith et al., 2017). Outside the CV, by contrast, GNSS VLM minima co-occur with TWS maxima (Fig. 6h, 6i), consistent with elastic crustal loading by seasonal water-mass variations (Argus et al., 2017; Carlson et al., 2022; Johnson et al., 2017). The high-resolution InSAR observations capture both regimes within a single dataset, with deformation peaks co-occurring with GWL in the valley interior and with TWS near the margins where the elastic loading signal dominates (Figs. 5b, 6j). The consistency of these phase relationships across multiple independent datasets, including groundwater wells (Fig. 4a), GNSS and InSAR deformation (Figs. 4b, 5), and GRACE-derived storage (Figs. 4g, 6g), indicates that they reflect a robust, system-scale response rather than artifacts of any individual dataset or method.

A further basin-scale indicator of mountain–groundwater connectivity is the near-complete disappearance of annual power in both snow storage and GRACE-derived groundwater storage during the severe drought years of 2007–2009 and 2012–2015, when Sierra Nevada snowpack was strongly reduced or absent (Figs. 1c, 3e, 3g). Other water storage components show reduced, but not absent, annual variability during the same periods. We interpret this co-disappearance as evidence that seasonal groundwater storage dynamics in the CV are tightly coupled to snowpack volume and subsequent snowmelt at the basin scale — a result that is notable given the difficulty of observing recharge processes across the full mountain–valley system. Snowmelt is likely relevant to both Mountain Front Recharge (MFR) and Mountain Block Recharge (MBR), with MFR more important for replenishing shallow, unconfined aquifers and MBR for transmitting water and pressure to deeper, semi-confined aquifers via fractures in the mountain block (Fig. 2). This interpretation does not by itself discriminate between shallow and deep recharge pathways, but it motivates the more specific analysis in Sections 4.2 and 4.3.

4.2 Pressure and Storage Propagation: In Concert or in Sequence?

A key finding of this study is that GRACE-derived GWS peaks approximately three months later than GWL in the CV (Fig. 6g, k). Because GWL and poroelastic surface deformation respond to changes in pore-fluid pressure, while GRACE measures bulk water mass integrated across shallow and deep aquifer systems, this phase lag indicates that the two observation types record fundamentally different aspects of aquifer dynamics. An earlier pressure response relative to a later storage response is physically expected when a pressure signal propagates through a hydraulically connected system ahead of the associated bulk flow of groundwater (Fetter & Kreamer, 2022) (see also Supplementary Text S2). Under this framework, seasonal increases in pore pressure within mountain aquifers driven by snowmelt infiltration can be transmitted through connected MBR and MFR pathways to modulate pressure conditions in deeper basin aquifers on relatively short timescales, even before a corresponding change in bulk groundwater storage is detectable by GRACE. The dry-season decline in mountain water

https://doi.org/10.5194/egusphere-2026-3061
Preprint. Discussion started: 11 June 2026

availability may then reduce groundwater flow from the preceding wet season, delaying the onset of a detectable storage change in the valley, such that pressure perturbations propagate into the basin aquifer system in advance of the storage signal. This pressure–storage distinction is essential for interpreting the timing relationships observed across datasets and supports a system-scale hydraulic connection between Sierra Nevada water availability and CV aquifer dynamics. We note, however, that the GWS estimate carries uncertainty because it is derived as a residual after correcting GRACE TWS for soil, snow, and reservoir storage contributions, and phase shifts in any of these corrections propagate into the inferred GWS timing. Our uncertainty analysis (Section 3.2; Figs. S12–S13) demonstrates that the three-month delay between GWS and GWL peaks remains robust across the plausible range of correction uncertainties, supporting the interpretation of distinct pressure- and storage-propagation processes. Nevertheless, this result should be treated as indicative rather than conclusive, and future studies using improved hydrological corrections and higher-resolution gravity data would help to better constrain the magnitude and timing of this lag.

4.3 Multi-Sensor Evidence for a Significant MBR from High-Mountains to Deep CV Aquifers

Together, the timing relationships described above are consistent with a hydraulic connection between high-mountain aquifers and deep CV aquifers via MBR pathways (Fig. 2). Previous studies have highlighted the importance of mountain system recharge but remain divided on the relative contributions of MBR and MFR at basin scales (Argus et al., 2022; Armengol et al., 2024; Gilbert & Maxwell, 2017; Schreiner-McGraw & Ajami, 2022). Our results provide regional-scale, multi-sensor observational evidence that is consistent with MBR playing a significant role in transmitting seasonal pressure signals to deep aquifer systems. We emphasize that our analysis identifies temporal relationships consistent with pressure propagation rather than directly quantifying recharge fluxes or distinguishing natural from anthropogenic contributions. Three independent lines of evidence support this interpretation.

First, the observed annual rise in GWL at deep well sites across the CV, including wells below the Corcoran Clay, requires a mechanism capable of transmitting positive pressure to confined aquifer layers on seasonal timescales. Direct vertical percolation of surface water through the low-permeability Corcoran Clay and regional clay-lens system is implausible at monthly to annual timescales (McMahon et al., 2011; Shirzaei et al., 2019), and groundwater pumping from deep confined aquifers can only explain an annual decline in GWL, not the observed rise. The annual increase in deep GWL therefore implies lateral pressure transmission from outside the confining unit, a signature consistent with MBR pathways connecting elevated mountain aquifers to deep valley aquifers (Fig. 2b).

Second, the high-resolution InSAR LOS deformation maps reveal an outward migration of the annual peak DOY from the center of the San Joaquin Valley toward its margins (Figs. 5b and S14), a pattern that persists consistently across wet and dry years. This at first appears to conflict with findings by Neely et al. (2021, 2024), who reported inward propagation of seasonal signals from the Sierra Nevada toward the valley center. However, both patterns are present in our results and reflect different recharge mechanisms operating at different spatial scales. The localized inward-propagating feature near the northeastern CV mountain front (Fig. 5b) closely matches the observations of Neely et al. (2021, 2024) and is consistent with MFR, where

https://doi.org/10.5194/egusphere-2026-3061
Preprint. Discussion started: 11 June 2026

surface water from Sierra Nevada streams contributes to aquifers near the mountain front. The broader, basin-scale outward migration identified here is not explained by MFR alone and instead reflects a system in which pressure changes propagate outward through hydraulically connected aquifer units from the valley center, where hydraulic head gradients are greatest due to sustained groundwater depletion, toward surrounding regions, consistent with fundamental principles of groundwater flow (Darcy's law; Supplementary Text S2). Because InSAR measures a vertically integrated signal across the aquifer system, it captures the combined signature of both mechanisms.

Third, the approximately one-and-a-half-month delay between peak mountain water availability (Fig. 6b) and peak GWL in the CV (Fig. 6k) provides a physically plausible time window for pressure transmission via MBR pathways. This lag is consistent with the pressure diffusion timescales estimated from our first-order model (Section 4.4) and with documented response times in other systems where snowmelt drives seasonal aquifer pressure responses in fractured bedrock environments (Montgomery-Brown et al., 2019; Saar & Manga, 2003).

4.4 Feasibility of the MBR Connection: First-order Pressure Diffusion Assessment

To assess whether the observed timing relationships are physically consistent with MBR, we apply a simplified one-dimensional pressure diffusion model (Section 2.5, Eq. 1 and S5) across the range of hydraulic diffusivity values reported for fractured crystalline bedrock (Saar & Manga, 2003; Gao et al., 2000; Montgomery-Brown et al., 2019). For a diffusivity of κ = 0.3 m²/s, representative of the Sierra Nevada's granitic bedrock, the estimated time for a seasonal pressure front to propagate vertically to depths of 600–2000 m, corresponding to the range of confined aquifer depths in the CV, is 18–36 days, broadly consistent with the observed one-to-two-month lag (Fig. 6b, 6k). Sensitivity tests spanning κ = 0.1–0.5 m²/s yield propagation times of 12–73 days at those depths (Fig. S16, S17), encompassing the observed delay within the uncertainty range. An additional horizontal flow component of 10 km through layers with diffusivities of 10–80 m²/s contributes an estimated 18–51 additional days of delay, which remains consistent with the total observed lag. We further note that the model has been successfully applied in an analogous setting to assess groundwater–surface water connectivity surrounding Lake Mead (Khorrami et al., 2025).

This model is intentionally simplified and does not account for vadose-zone processes, fracture-network heterogeneity, three-dimensional flow geometry, or complex storage behavior arising from secondary porosity in fractured aquifers. While vadose-zone dynamics may locally modify the timing of recharge in the mountain block, our analysis focuses on regional-scale phase relationships derived from multiple observational datasets, and the fundamental observation of a consistent lag between mountain water availability and deep aquifer response is not altered by such local modifications. Accordingly, the diffusion analysis should be interpreted as a feasibility assessment, demonstrating that the observed delays are physically plausible given reasonable hydraulic properties, rather than a predictive quantification of MBR fluxes. Future work using fully coupled three-dimensional hydrogeologic models with constrained diffusivity estimates from field campaigns and geophysical observations (Viswanathan et al., 2022) will be needed to move from plausibility to prediction.

https://doi.org/10.5194/egusphere-2026-3061
Preprint. Discussion started: 11 June 2026

4.5 Uncertainties and Limitations

Several sources of uncertainty affect our results and should be considered when interpreting the conclusions. With respect to the observational datasets, the wavelet time-frequency analysis is sensitive to data gaps and variable sampling rates, as with other spectral methods (Goswami & Chan, 1999), though the continuous wavelet transform's time-frequency localization minimizes error propagation relative to Fourier-based approaches. GNSS time series may be contaminated by non-tidal loading, thermoelastic deformation, tectonic signals, and draconitic errors that can produce spurious annual oscillations (Chanard et al., 2020); our selection criterion of retaining only stations with seasonal amplitudes exceeding their time-series noise level reduces but does not eliminate this risk. The GWS time series derived from GRACE carries uncertainties inherited from the correction terms (SoS, SnS, ReS), yet the three-month delay between GWS and GWL peaks is robust against plausible phase uncertainties in those corrections (Section 3.2; Figs. S12–S13). The number of deep observation wells in the southern San Joaquin Valley is low (22 sites below the Corcoran Clay); however, we prioritized data quality and representativeness of confined aquifer conditions over spatial density, and the timing of GWL peaks shows low interannual variability across available sites (Fig. S9), supporting the reliability of our spatial averages.

Groundwater pumping represents the most significant anthropogenic confound on our interpretations. Seasonal pumping in the CV typically begins in spring, overlapping with the period of declining GWL (Fig. 4a), and may alter hydraulic gradients between the valley and the surrounding highlands. This could reduce the apparent lag between mountain water availability and GWL response, such that the observed one-and-a-half-month delay likely represents an upper bound on the natural system response time. While we minimized pumping artifacts by focusing on observation wells rather than production wells and on regional-scale rather than local signals, the data do not permit full isolation of natural recharge from anthropogenic influences in this heavily managed system.

For the pressure diffusion model, the Skempton coefficient for poroelastic stress transfer from surface loading is orders of magnitude smaller than direct pore-pressure changes for semi-confined aquifers (Wang, 2000; Zhai et al., 2019), and this contribution is therefore neglected. The key source of model uncertainty is the hydraulic diffusivity of the fractured mountain block, which is poorly constrained at regional scales due to limited knowledge of fracture extent and depth. Our sensitivity tests (Fig. S16, S17) span a representative range of published values, and the estimated diffusion times remain consistent with the observed lag across this range. But more detailed textural information about the mountain block, e.g., from extensive and innovative field campaigns, and validation via hydrological model experiments assimilating geodetic and hydrological observations would improve the constraint on this parameter (Smith & Knight, 2019; Viswanathan et al., 2022).

Finally, our analysis does not consider the effects of climate extremes, such as years dominated by atmospheric rivers, which Siirila-Woodburn et al. (2023) suggest may result in lower aquifer recharge relative to snowmelt-dominated years. The overall impact of such events on recharge to deep confined aquifers remains unclear in the absence of coupled mesoscale models integrating general circulation models with hydrogeological simulations (Smerdon, 2017), and this represents an important

https://doi.org/10.5194/egusphere-2026-3061
Preprint. Discussion started: 11 June 2026

direction for future work as extreme events are projected to increase in frequency and intensity throughout the 21st century (AghaKouchak et al., 2020).

5. Summary & Outlook

Recent studies have recognized mountains' critical role in freshwater supply to lowland dry basins, debunking the outdated notion that mountain groundwater storage and supply are negligible (Ajami et al., 2011; Markovich et al., 2019; Meixner et al., 2016; Somers & McKenzie, 2020; Wahi et al., 2008; Welch & Allen, 2014). Our study adds basin-scale observational evidence that high-mountain hydrologic processes, including snow accumulation and melt, are linked to seasonal groundwater dynamics in the CV. In addition, we provide further evidence for the relevance of MBR. Both findings have significant implications for replenishing groundwater resources, particularly in aquifer basins located in arid and semi-arid regions and adjacent to mountains, such as the Adelaide Plains basin, South Australia (Bresciani et al., 2018), Upper San Pedro Basin and Sabino Creek, Arizona, USA (Ajami et al., 2011; Wahi et al., 2008) and CV California, emphasizing the complementary role of focused groundwater recharge through river channels, diffuse recharge via mountain front systems and diffuse recharge via fractured deep bedrocks. Our findings further highlight the importance of considering pressure dynamics, in addition to storage changes, when interpreting groundwater observations at seasonal time scales. The results suggest that high-mountain hydrologic processes can influence deep-basin aquifers through mechanisms not fully captured in current large-scale hydrological models.

We use a data-driven approach that does not include detailed physical process simulations. The first-order 1D-pressure propagation model is intended to demonstrate the general feasibility of the MBR via direct hydraulic connectivity between the Sierra Nevada and deep CV aquifers, rather than to quantify MBR fluxes, and we think it is well supported by the hydrological and geodetic observations we presented. Similarly, existing geodetic estimates, such as those of Argus et al. (2022), infer MBR indirectly as the difference between gravity- and elastic-loading-based annual GWS estimates and hydrological model output that excludes MSR. Because this approach cannot discriminate MBR from MFR, such residual estimates should not be interpreted as MBR alone.

Reliably quantifying MBR at the scale of the CV and distinguishing it from MFR will require fully coupled 3D fluid-solid media groundwater models that account for groundwater flow (Schreiner-McGraw & Ajami, 2022) but also integrate the wealth of hydrologic, geodetic, geophysical, and remote sensing observations sensitive to the dynamics in the aquifers, as demonstrated in this study. These model experiments should be cross-checked and absorb independent constraints from isogeochemical characterizations (e.g., (Armengol et al., 2024; Earman et al., 2006)) and advances in geophysical observations (Knight et al., 2022; Smith & Knight, 2019). Detailed model experiments will also help to determine the human impact, i.e., via pumping and managed aquifer recharge, on the various aquifer recharge fluxes, which we cannot specify with the presented observations alone.

https://doi.org/10.5194/egusphere-2026-3061
Preprint. Discussion started: 11 June 2026

Incorporating mountain-block recharge and pressure propagation into hydroclimatic and groundwater models may improve predictions of water availability in snowmelt-dominated regions, particularly under changing climate conditions. More comprehensive studies integrating multi-sensor observations with coupled hydrogeologic models are needed to further quantify these processes and their implications for sustainable groundwater management.

Data Availability

All data used for this study are publicly available from the following sources. GRACE JPL Mascon data were accessed from JPL PO.DAAC (Wiese et al., 2019). SNODAS data were downloaded from the National Snow & Ice Data Center (NOHRSC, 2004). GLDAS model outputs for Noah, CLSM, and VIC were retrieved from the Goddard Earth Sciences Data and Information Services Center (Beaudoing et al., 2016). We kindly thank Hannes Müller Schmied (hannes.mueller.schmied@em.uni-frankfurt.de) at the University of Frankfurt for providing WGHM version 2.2d outputs. GNSS time series were downloaded from the Nevada Geodetic Laboratory (Blewitt et al., 2018). The California Department of Water Resources provides reservoir data (CDWR, 2017) and groundwater level data. We retrieved all groundwater well sites within the study area as a bulk download from the California Natural Resources Agency via the California Open Data Portal for "Periodic Groundwater Level Measurements" (CDWR, 2019b) and for "Continuous Groundwater Level Measurements" (CDWR, 2019a). Further, we collected all available groundwater level data for the study region from the USGS archives (USGS, 2021) under the categories "Daily Data" and "Field Measurements". Open-source wavelet software packages were retrieved by C. Torrence and G. Compo (Torrence & Compo, 1998) and by Erickson (Erickson, 2019). InSAR results, assembled groundwater records, and all data analysis results are presented in the supporting information or figures. They are also available as data files in the Virginia Tech Data Repository (*to be defined*).

Author contribution

SW contributed to the conceptualization, methodology, investigation, visualization, supervision, and writing of the original draft as well as review and editing of the manuscript. MS contributed to the conceptualization, methodology, investigation, and review and editing of the manuscript. GC contributed to the investigation. GC and RB contributed to the review and editing of the manuscript.

Competing interests

The authors declare that they have no conflict of interest.

https://doi.org/10.5194/egusphere-2026-3061
Preprint. Discussion started: 11 June 2026

Acknowledgments

We thank reviewers and editors for their constructive comments and suggestions. This research was partly funded by the National Aeronautics and Space Administration grants NNX17AD98G (SW, MS, GC), 80NSSC21K0419 (SW, MS, GC), and 80NSSC21K0061 (SW), as well as the Department of Energy grant DE-SC0019307 (MS). OpenAI's ChatGPT (GPT-5.5 Thinking) was used to support editorial refinement of the manuscript. The authors reviewed and approved all AI-assisted edits.

References

Adusumilli, S., Borsa, A. A., Fish, M. A., McMillan, H. K., & Silverii, F. (2019). A decade of terrestrial water storage changes across the contiguous United States from GPS and GRACE. *Geophysical Research Letters*, 2019GL085370. https://doi.org/10.1029/2019GL085370

AghaKouchak, A., Chiang, F., Huning, L. S., Love, C. A., Mallakpour, I., Mazdiyasni, O., Moftakhari, H., Papalexiou, S. M., Ragno, E., & Sadegh, M. (2020). Climate Extremes and Compound Hazards in a Warming World. *Annual Review of Earth and Planetary Sciences*, *48*.

Ajami, H., Troch, P. A., Maddock, T., Meixner, T., & Eastoe, C. (2011). Quantifying mountain block recharge by means of catchment-scale storage-discharge relationships. *Water Resources Research*, *47*(4). https://doi.org/10.1029/2010WR009598

Alam, S., Gebremichael, M., Ban, Z., Scanlon, B. R., Senay, G., & Lettenmaier, D. P. (2021). Post-Drought Groundwater Storage Recovery in California's Central Valley. *Water Resources Research*, *57*(10). https://doi.org/10.1029/2021WR030352

Alley, W. M. (2002). Flow and Storage in Groundwater Systems. *Science*, *296*(5575), 1985–1990. https://doi.org/10.1126/science.1067123

Argus, D. F., Landerer, F. W., Wiese, D. N., Martens, H. R., Fu, Y., Famiglietti, J. S., Thomas, B. F., Farr, T. G., Moore, A. W., & Watkins, M. M. (2017). Sustained water loss in California's mountain ranges during severe drought from 2012 to 2015 inferred from GPS. *Journal of Geophysical Research: Solid Earth*, *122*(12), 10,510-559,585. https://doi.org/10.1002/2017JB014424

Argus, D. F., Martens, H. R., Borsa, A. A., Knappe, E., Wiese, D. N., Alam, S., Anderson, M., Khatiwada, A., Lau, N., Peidou, A., Swarr, M., White, A., Bos, M. S., Landerer, F. W., & Gardner, P. (2022). Subsurface water flux in California's Central Valley and its source watershed from space geodesy. *Geophysical Research Letters*. https://doi.org/10.1029/2022GL099583

Armengol, S., Ajami, H., Acero Triana, J. S., O. Sickman, J., & Ortega, L. (2024). Isogeochemical Characterization of Mountain System Recharge Processes in the Sierra Nevada, California. *Water Resources Research*, *60*(7). https://doi.org/10.1029/2023WR035719

https://doi.org/10.5194/egusphere-2026-3061
Preprint. Discussion started: 11 June 2026

Ayres, A., Hanak, E., Gray, B., Sencan, G., Bruno, E., Bou, A. E., & Collins, J. (2021). *Improving California' s Water Market*. https://www.ppic.org/publication/improving-californias-water-market/

Bales, R. C., Hopmans, J. W., O'Geen, A. T., Meadows, M., Hartsough, P. C., Kirchner, P., Hunsaker, C. T., & Beaudette, D. (2011). Soil Moisture Response to Snowmelt and Rainfall in a Sierra Nevada Mixed-Conifer Forest. *Vadose Zone Journal*, *10*(3), 786–799. https://doi.org/10.2136/vzj2011.0001

Beaudoing, H., Rodell, M., & NASA/GSFC/HSL. (2016). GLDAS Noah Land Surface Model L4 monthly 0.25 x 0.25 degree V2.1 [Dataset]. *Greenbelt, Maryland, USA, Goddard Earth Sciences Data and Information Services Center (GES DISC), Date Accessed: 2021-12-23*. https://doi.org/10.5067/SXAVCZFAQLNO

Blewitt, G., Hammond, W., & Kreemer, C. (2018). Harnessing the GPS Data Explosion for Interdisciplinary Science [Dataset]. *Eos, Date Accessed 2023-02-09*, *99*. https://doi.org/10.1029/2018EO104623

Borsa, A. A., Agnew, D. C., & Cayan, D. R. (2014). Ongoing drought-induced uplift in the western United States. *Science*, *345*(6204), 1587–1590. https://doi.org/10.1126/science.1260279

Bresciani, E., Cranswick, R. H., Banks, E. W., Batlle-Aguilar, J., Cook, P. G., & Batelaan, O. (2018). Using hydraulic head, chloride and electrical conductivity data to distinguish between mountain-front and mountain-block recharge to basin aquifers. *Hydrology and Earth System Sciences*, *22*(2), 1629–1648. https://doi.org/10.5194/hess-22-1629-2018

Brush, C. F., Dogrul, E. C., & Kadir, T. N. (2013). Development and Calibration of the California Central Valley Groundwater-Surface Water Simulation Model (C2VSim), Version 3.02-CG. In *California Department of Water Resources Technical Memorandum* (DWR Technical Memorandum). California Department of Water Resources. http://baydeltaoffice.water.ca.gov/modeling/hydrology/c2vsim/index_c2vsim.cfm

Bürgmann, R., Chanard, K., & Fu, Y. (2024). Climate- and weather-driven solid Earth deformation and seismicity. In *GNSS Monitoring of the Terrestrial Environment* (pp. 257–285). Elsevier. https://doi.org/10.1016/B978-0-323-95507-2.00011-6

Burow, K. R., Dubrovsky, N. M., & Shelton, J. L. (2007). Temporal trends in concentrations of DBCP and nitrate in groundwater in the eastern San Joaquin Valley, California, USA. *Hydrogeology Journal*, *15*(5), 991–1007. https://doi.org/10.1007/s10040-006-0148-7

Carlson, G., Shirzaei, M., Ojha, C., & Werth, S. (2020). Subsidence-Derived Volumetric Strain Models for Mapping Extensional Fissures and Constraining Rock Mechanical Properties in the San Joaquin Valley, California. *Journal of Geophysical Research: Solid Earth*. https://doi.org/10.1029/2020JB019980

Carlson, G., Shirzaei, M., Werth, S., Zhai, G., & Ojha, C. (2020). Seasonal and Long-Term Groundwater Unloading in the Central Valley Modifies Crustal Stress. *Journal of Geophysical Research: Solid Earth*, *125*(1), 1–17. https://doi.org/10.1029/2019JB018490

Carlson, G., Werth, S., & Shirzaei, M. (2022). Joint Inversion of GNSS and GRACE for Terrestrial Water Storage Change in California. *Journal of Geophysical Research: Solid Earth*, *127*(3). https://doi.org/10.1029/2021JB023135

https://doi.org/10.5194/egusphere-2026-3061
Preprint. Discussion started: 11 June 2026

Carlson, G., Werth, S., & Shirzaei, M. (2024). A novel hybrid GNSS, GRACE, and InSAR joint inversion approach to constrain water loss during a record-setting drought in California. *Remote Sensing of Environment*, *311*, 114303. https://doi.org/10.1016/j.rse.2024.114303

CDWR. (2017). *California Department of Water Resources, California Data Exchange Center, Active Monthly Reservoirs [Dataset]*. Data Accessed 2020-11-22. http://cdec.water.ca.gov/misc/monthly_res.html

CDWR. (2019a). *Continuous Groundwater Level Measurements [Dataset]*. Date Accessed 2019-12-18. https://data.ca.gov/dataset/continuous-groundwater-level-measurements

CDWR. (2019b). *Periodic Groundwater Level Measurements, California Department of Water Resources [Dataset]*. Date Accessed 2019-12-18. https://data.cnra.ca.gov/dataset/periodic-groundwater-level-measurements

Costantini, M. (1998). A novel phase unwrapping method based on network programming. *IEEE Transactions on Geoscience and Remote Sensing*, *36*(3), 813–821. https://doi.org/10.1109/36.673674

Dillon, P. (2005). Future management of aquifer recharge. *Hydrogeology Journal*, *13*(1), 313–316. https://doi.org/10.1007/s10040-004-0413-6

Earman, S., Campbell, A. R., Phillips, F. M., & Newman, B. D. (2006). Isotopic exchange between snow and atmospheric water vapor: Estimation of the snowmelt component of groundwater recharge in the southwestern United States. *Journal of Geophysical Research Atmospheres*, *111*(9). https://doi.org/10.1029/2005JD006470

Erickson, J. (2019). *Continuous wavelet transform and inverse [Software]* (Retrieved August 30, 2019.). MATLAB Central File Exchange. https://www.mathworks.com/matlabcentral/fileexchange/20821-continuous-wavelet-transform-and-inverse

Escriva-Bou, A., Hui, R., Maples, S., Medellín-Azuara, J., Harter, T., & Lund, J. R. (2020). Planning for groundwater sustainability accounting for uncertainty and costs: An application to California's Central Valley. *Journal of Environmental Management*, *264*, 110426.

Escriva-Bou, A., Sencan, G., & Hanak, E. (2021). *Groundwater Recharge, Fact Sheet August 2021*. https://www.ppic.org/publication/groundwater-recharge/

Famiglietti, J. S., Lo, M., Ho, S. L., Bethune, J., Anderson, K. J., Syed, T. H., Swenson, S. C., de Linage, C. R., & Rodell, M. (2011). Satellites measure recent rates of groundwater depletion in California's Central Valley. *Geophysical Research Letters*, *38*(3). https://doi.org/10.1029/2010GL046442

Farr, T. G., Rosen, P. A., Caro, E., Crippen, R., Duren, R., Hensley, S., Kobrick, M., Paller, M., Rodriguez, E., Roth, L., Seal, D., Shaffer, S., Shimada, J., Umland, J., Werner, M., Oskin, M., Burbank, D., & Alsdorf, D. (2007). The Shuttle Radar Topography Mission. *Reviews of Geophysics*, *45*(2), RG2004. https://doi.org/10.1029/2005RG000183

Faunt, C. C. (2009). *Groundwater Availability of the Central Valley Aquifer, California* (C. C. Faunt, Ed.). U.S. Geological Survey Professional Paper 1766. https://pubs.usgs.gov/pp/1766/

Faunt, C. C., Sneed, M., Traum, J., & Brandt, J. T. (2016). Water availability and land subsidence in the Central Valley, California, USA. *Hydrogeology Journal*, *24*(3), 675–684. https://doi.org/10.1007/s10040-015-1339-x

https://doi.org/10.5194/egusphere-2026-3061
Preprint. Discussion started: 11 June 2026

Feth, J. H. (1964). Hidden Recharge. *Groundwater*, *2*(4), 14–17. https://doi.org/10.1111/j.1745-6584.1964.tb01780.x

Fetter, C. W., & Kreamer, D. (2022). *Applied Hydrogeology* (5th ed.). Waveland Press.

Fox-Kemper, B., Hewitt, H. T., Xiao, C., Aðalgeirsdóttir, G., Drijfhout, S. S., Edwards, T. L., Golledge, N. R., Hemer, M., Kopp, R. E., Krinner, G., Mix, A., Notz, D., Nowicki, S., Nurhati, I. S., Ruiz, L., Sallée, J.-B., Slangen, A. B. A., & Yu, Y. (2021). Ocean, Cryosphere and Sea Level Change. In *Climate Change 2021: The Physical Science Basis. Contribution of Working Group I to the Sixth Assessment Report of the Intergovernmental Panel on Climate Change [MassonDelmotte, et al. (eds.)]*. Cambridge University Press. https://doi.org/10.1017/9781009157896

Franceschetti, G., & Lanari, R. (1999). *Synthetic aperture radar processing*. CRC Press.

Galloway, D. L., Jones, D. R., & Ingebritsen, S. E. (1999). *Land subsidence in the United States*. U.S. Geological Survey Circular 1182. https://doi.org/10.3133/cir1182

Galloway, D. L., Jones, D. R., & Ingebritsen, S. E. (2000). Land Subsidence in the United States: U.S. Geological Survey Fact Sheet 165-00. *U.S. Geological Survey Fact Sheet 165-00*, (December), 4. http://water.usgs.gov/ogw/pubs/fs00165/SubsidenceFS.v7.PDF

Ghasemizade, M., Asante, K. O., Petersen, C., Kocis, T., Dahlke, H. E., & Harter, T. (2019). An Integrated Approach Toward Sustainability via Groundwater Banking in the Southern Central Valley, California. *Water Resources Research*, *55*(4), 2742–2759. https://doi.org/10.1029/2018WR024069

Gilbert, J. M., & Maxwell, R. M. (2017). Examining regional groundwater-surface water dynamics using an integrated hydrologic model of the San Joaquin River basin. *Hydrology and Earth System Sciences*, *21*(2), 923–947. https://doi.org/10.5194/hess-21-923-2017

Goswami, J. C., & Chan, A. K. (1999). *Fundamentals of Wavelets: Theory, Algorithms, and Applications*. Wiley-Interscience.

Hanak, E., Lund, J., Arnold, B., Escriva-Bou, A., Gray, B., Green, S., Harter, T., Howitt, R., MacEwan, D., & Medellín-Azuara, J. (2017). *Water Stress and a Changing San Joaquin Valley*. Public Policy Institute of California. https://www.ppic.org/publication/water-stress-and-a-changing-san-joaquin-valley/

Hanson, R. T., Flint, L. E., Flint, A. L., Dettinger, M. D., Faunt, C. C., Cayan, D., & Schmid, W. (2012). A method for physically based model analysis of conjunctive use in response to potential climate changes. *Water Resources Research*, *48*(2). https://doi.org/10.1029/2011WR010774

Harpold, A., Dettinger, M., & Rajagopal, S. (2017). Defining Snow Drought and Why It Matters. *Eos*. https://doi.org/10.1029/2017EO068775

Hatchett, B. J., & McEvoy, D. J. (2018). Exploring the origins of snow drought in the northern sierra nevada, california. *Earth Interactions*, *22*(2), 1–13. https://doi.org/10.1175/EI-D-17-0027.1

Herrera-García, G., Ezquerro, P., Tomás, R., Béjar-Pizarro, M., López-Vinielles, J., Rossi, M., Mateos, R. M., Carreón-Freyre, D., Lambert, J., Teatini, P., Cabral-Cano, E., Erkens, G., Galloway, D., Hung, W.-C. C., Kakar, N., Sneed, M., Tosi, L., Wang, H., Ye, S., … Ye, S. (2021). Mapping the global threat of land subsidence. *Science*, *371*(6524), 34–36. https://doi.org/10.1126/science.abb8549

https://doi.org/10.5194/egusphere-2026-3061
Preprint. Discussion started: 11 June 2026

Huth, A. K., Leydecker, A., Sickman, J. O., & Bales, R. C. (2004). A two-component hydrograph separation for three high-elevation catchments in the Sierra Nevada, California. *Hydrological Processes*, *18*(9), 1721–1733. https://doi.org/10.1002/hyp.1414

Jakeman, A. J., Barreteau, O., Hunt, R. J., Rinaudo, J.-D., Ross, A., Arshad, M., & Hamilton, S. (2016). Integrated Groundwater Management: An Overview of Concepts and Challenges. In *Integrated Groundwater Management* (pp. 3–20). Springer International Publishing. https://doi.org/10.1007/978-3-319-23576-9_1

Jaramillo, F., Aminjafari, S., Castellazzi, P., Fleischmann, A., Fluet-Chouinard, E., Hashemi, H., Hubinger, C., Martens, H. R., Papa, F., Schöne, T., Tarpanelli, A., Virkki, V., Wang-Erlandsson, L., Abarca-del-Rio, R., Borsa, A., Destouni, G., Di Baldassarre, G., Moore, M., Posada-Marín, J. A., … Salazar, J. F. (2024). The Potential of Hydrogeodesy to Address Water-Related and Sustainability Challenges. *Water Resources Research*, *60*(11). https://doi.org/10.1029/2023WR037020

Jasechko, S., Seybold, H., Perrone, D., Fan, Y., Shamsudduha, M., Taylor, R. G., Fallatah, O., & Kirchner, J. W. (2024). Rapid groundwater decline and some cases of recovery in aquifers globally. *Nature* |, *625*, 715. https://doi.org/10.1038/s41586-023-06879-8

Jódar, J., Cabrera, J. A., Martos-Rosillo, S., Ruiz-Constán, A., González-Ramón, A., Lambán, L. J., Herrera, C., & Custodio, E. (2017). Groundwater discharge in high-mountain watersheds: A valuable resource for downstream semi-arid zones. The case of the Bérchules River in Sierra Nevada (Southern Spain). *Science of The Total Environment*, *593–594*, 760–772. https://doi.org/10.1016/j.scitotenv.2017.03.190

Johnson, C. W., Fu, Y., & Bürgmann, R. (2017). Seasonal water storage, stress modulation, and California seismicity. *Science*, *356*(6343), 1161–1164. https://doi.org/10.1126/science.aak9547

Khorrami, M., Werth, S., Zehsaz, S., & Shirzaei, M. (2025). Drought-induced changes in groundwater-surface water exchange at Lake Mead area. *Journal of Hydrology: Regional Studies*, *62*, 102996. https://doi.org/10.1016/j.ejrh.2025.102996

Knight, R., Steklova, K., Miltenberger, A., Kang, S., Goebel, M., & Fogg, G. (2022). Airborne geophysical method images fast paths for managed recharge of California's groundwater. *Environmental Research Letters*, *17*(12), 124021. https://doi.org/10.1088/1748-9326/aca344

Konikow, L. F. (2015). Long-Term Groundwater Depletion in the United States. *Groundwater*, *53*(1), 2–9. https://doi.org/10.1111/gwat.12306

Kourakos, G., Brunetti, G., Bigelow, D. P., Wallander, S., & Dahlke, H. E. (2023). Optimizing Managed Aquifer Recharge Locations in California's Central Valley Using an Evolutionary Multi-Objective Genetic Algorithm Coupled With a Hydrological Simulation Model. *Water Resources Research*, *59*(5). https://doi.org/10.1029/2022WR034129

Kourakos, G., Dahlke, H. E., & Harter, T. (2019). Increasing Groundwater Availability and Seasonal Base Flow Through Agricultural Managed Aquifer Recharge in an Irrigated Basin. *Water Resources Research*, *55*(9), 7464–7492. https://doi.org/10.1029/2018WR024019

https://doi.org/10.5194/egusphere-2026-3061
Preprint. Discussion started: 11 June 2026

Lee, J.-C., & Shirzaei, M. (2023). Novel algorithms for pair and pixel selection and atmospheric error correction in multitemporal InSAR. *Remote Sensing of Environment*, *286*, 113447. https://doi.org/10.1016/j.rse.2022.113447

Li, R., Ou, G., Pun, M., & Larson, L. (2018). Evaluation of Groundwater Resources in Response to Agricultural Management Scenarios in the Central Valley, California. *Journal of Water Resources Planning and Management*, *144*(12), 04018078. https://doi.org/10.1061/(asce)wr.1943-5452.0001014

Liu, F., Conklin, M. H., & Shaw, G. D. (2017). Insights into hydrologic and hydrochemical processes based on concentration-discharge and end-member mixing analyses in the mid-Merced River Basin, Sierra Nevada, California. *Water Resources Research*, *53*(1), 832–850. https://doi.org/10.1002/2016WR019437

Madani, K. (2026). *Global Water Bankruptcy: Living Beyond Our Hydrological Means in the Post Crisis Era*. https://doi.org/10.53328/INR26KAM001

Markovich, K. H., Manning, A. H., Condon, L. E., & McIntosh, J. C. (2019). Mountain-Block Recharge: A Review of Current Understanding. *Water Resources Research*, *55*(11), 8278–8304. https://doi.org/10.1029/2019WR025676

Marwaha, N., Kourakos, G., Levintal, E., & Dahlke, H. E. (2021). Identifying Agricultural Managed Aquifer Recharge Locations to Benefit Drinking Water Supply in Rural Communities. *Water Resources Research*, *57*(3). https://doi.org/10.1029/2020WR028811

Massoud, E. C., Purdy, A. J., Miro, M. E., & Famiglietti, J. S. (2018). Projecting groundwater storage changes in California's Central Valley. *Scientific Reports*, *8*(1), 12917. https://doi.org/10.1038/s41598-018-31210-1

McCabe, G. J., Palecki, M. A., & Betancourt, J. L. (2004). Pacific and Atlantic Ocean influences on multidecadal drought frequency in the United States. *Proceedings of the National Academy of Sciences*, *101*(12), 4136–4141. https://doi.org/10.1073/pnas.0306738101

McMahon, P. B., Plummer, L. N., Böhlke, J. K., Shapiro, S. D., & Hinkle, S. R. (2011). A comparison of recharge rates in aquifers of the United States based on groundwater-age data. *Hydrogeology Journal*, *19*(4), 779–800. https://doi.org/10.1007/s10040-011-0722-5

Meixner, T., Manning, A. H., Stonestrom, D. A., Allen, D. M., Ajami, H., Blasch, K. W., Brookfield, A. E., Castro, C. L., Clark, J. F., & Gochis, D. J. (2016). Implications of projected climate change for groundwater recharge in the western United States. *Journal of Hydrology*, *534*, 124–138.

Meles, M. B., Bradford, S., Casillas-Trasvina, A., Chen, L., Osterman, G., Hatch, T., Ajami, H., Crompton, O., Levers, L., & Kisekka, I. (2024). Uncovering the gaps in managed aquifer recharge for sustainable groundwater management: A focus on hillslopes and mountains. In *Journal of Hydrology* (Vol. 639). Elsevier B.V. https://doi.org/10.1016/j.jhydrol.2024.131615

Meyer, P. L. (1970). *Introductory Probability and Statistical Applicaitons* (2nd ed.). Oxford & IBH Publishing Co.

Montgomery-Brown, E. K., Shelly, D. R., & Hsieh, P. A. (2019). Snowmelt-Triggered Earthquake Swarms at the Margin of Long Valley Caldera, California. *Geophysical Research Letters*, *46*(7), 3698–3705. https://doi.org/10.1029/2019GL082254

https://doi.org/10.5194/egusphere-2026-3061
Preprint. Discussion started: 11 June 2026

Mote, P. W., Li, S., Lettenmaier, D. P., Xiao, M., & Engel, R. (2018). Dramatic declines in snowpack in the western US. *Npj Climate and Atmospheric Science*, *1*(1). https://doi.org/10.1038/s41612-018-0012-1

Neely, W. R., Borsa, A. A., Burney, J. A., Levy, M. C., Silverii, F., & Sneed, M. (2021). Characterization of Groundwater Recharge and Flow in California's San Joaquin Valley From InSAR-Observed Surface Deformation. *Water Resources Research*, *57*(4), 1–20. https://doi.org/10.1029/2020wr028451

Neely, W. R., Knight, R., Kang, S., & Goebel, M. (2024). Exploring the InSAR signature associated with river-sourced recharge in California's San Joaquin Valley. *Environmental Research Letters*. https://doi.org/10.1088/1748-9326/ad5855

NOHRSC. (2004). *National Operational Hydrologic Remote Sensing Center, Snow Data Assimilation System (SNODAS) data products at NSIDC. Version 1. [Dataset]*. National Snow and Ice Data Center, Boulder, CO, USA, Date Accessed 2020-11-21. https://doi.org/10.7265/N5TB14TC

Ojha, C., Shirzaei, M., Werth, S., Argus, D. F., & Farr, T. G. (2018). Sustained Groundwater Loss in California's Central Valley Exacerbated by Intense Drought Periods. *Water Resources Research*, *54*(7), 4449–4460. https://doi.org/10.1029/2017WR022250

Ojha, C., Werth, S., & Shirzaei, M. (2019). Groundwater Loss and Aquifer System Compaction in San Joaquin Valley During 2012–2015 Drought. *Journal of Geophysical Research: Solid Earth*, *124*(3), 3127–3143. https://doi.org/10.1029/2018JB016083

Pepin, N., Bradley, R. S., Diaz, H. F., Baraer, M., Caceres, E. B., Forsythe, N., Fowler, H., Greenwood, G., Hashmi, M. Z., Liu, X. D., Miller, J. R., Ning, L., Ohmura, A., Palazzi, E., Rangwala, I., Schöner, W., Severskiy, I., Shahgedanova, M., Wang, M. B., … Yang, D. Q. (2015). Elevation-dependent warming in mountain regions of the world. *Nature Climate Change*, *5*(5), 424–430. https://doi.org/10.1038/nclimate2563

Perrone, D., & Jasechko, S. (2019). Deeper well drilling an unsustainable stopgap to groundwater depletion. *Nature Sustainability*, *2*(8), 773–782. https://doi.org/10.1038/s41893-019-0325-z

Quiring, S. M., & Goodrich, G. B. (2008). Nature and causes of the 2002 to 2004 drought in the southwestern United States compared with the historic 1953 to 1957 drought. *Climate Research*, *36*(1), 41–52. https://doi.org/10.3354/cr00735

Rodell, M., Houser, P. R., Jambor, U., Gottschalck, J., Mitchell, K., Meng, C.-J., Arsenault, K., Cosgrove, B., Radakovich, J., Bosilovich, M., Entin*, J. K., Walker, J. P., Lohmann, D., & Toll, D. (2004). The Global Land Data Assimilation System. *Bulletin of the American Meteorological Society*, *85*(3), 381–394. https://doi.org/10.1175/BAMS-85-3-381

Saar, M. O., & Manga, M. (2003). Seismicity induced by seasonal groundwater recharge at Mt. Hood, Oregon. *Earth and Planetary Science Letters*, *214*(3–4), 605–618. https://doi.org/10.1016/S0012-821X(03)00418-7

Scanlon, B. R., Longuevergne, L., & Long, D. (2012). Ground referencing GRACE satellite estimates of groundwater storage changes in the California Central Valley, USA. *Water Resources Research*, *48*(4), W04520. https://doi.org/10.1029/2011WR011312

https://doi.org/10.5194/egusphere-2026-3061
Preprint. Discussion started: 11 June 2026

Schmidt, R., Flechtner, F., Meyer, U., Neumayer, K.-H., Dahle, C., König, R., & Kusche, J. (2008). Hydrological Signals Observed by the GRACE Satellites. *Surveys in Geophysics*, *29*(4–5), 319–334. https://doi.org/10.1007/s10712-008-9033-3

Schreiner-McGraw, A. P., & Ajami, H. (2022). Combined impacts of uncertainty in precipitation and air temperature on simulated mountain system recharge from an integrated hydrologic model. *Hydrology and Earth System Sciences*, *26*(4), 1145–1164. https://doi.org/10.5194/hess-26-1145-2022

Shirzaei, M. (2013). A Wavelet-Based Multitemporal DInSAR Algorithm for Monitoring Ground Surface Motion. *Ieee Geoscience and Remote Sensing Letters*, *10*(3), 456–460. https://doi.org/10.1109/Lgrs.2012.2208935

Shirzaei, M., Bürgmann, R., & Fielding, E. J. (2017). Applicability of Sentinel-1 Terrain Observation by Progressive Scans multitemporal interferometry for monitoring slow ground motions in the San Francisco Bay Area. *Geophysical Research Letters*, *44*(6), 2733–2742. https://doi.org/10.1002/2017GL072663.

Shirzaei, M., Bürgmann, R., Foster, J., Walter, T. R., & Brooks, B. A. (2013). Aseismic deformation across the Hilina fault system, Hawaii, revealed by wavelet analysis of InSAR and GPS time series. *Earth and Planetary Science Letters*, *376*, 12–19. https://doi.org/10.1016/j.epsl.2013.06.011

Shirzaei, M., Ojha, C., Werth, S., Carlson, G., & Vivoni, E. R. (2019). Comment on "Short-lived pause in Central California subsidence after heavy winter precipitation of 2017" by K. D. Murray and R. B. Lohman. *Science Advances*, *5*(eaav8038). https://doi.org/10.1126/sciadv.aav8038

Siebert, S., Burke, J., Faures, J. M., Frenken, K., Hoogeveen, J., Döll, P., & Portmann, F. T. (2010). Groundwater use for irrigation - A global inventory. *Hydrology and Earth System Sciences*, *14*(10), 1863–1880. https://doi.org/10.5194/hess-14-1863-2010

Siirila-Woodburn, E. R., Dennedy-Frank, P. J., Rhoades, A., Vahmani, P., Maina, F., Hatchett, B., Zhou, Y., & Jones, A. (2023). The Role of Atmospheric Rivers on Groundwater: Lessons Learned From an Extreme Wet Year. *Water Resources Research*, *59*(6). https://doi.org/10.1029/2022WR033061

Siirila-Woodburn, E. R., Rhoades, A. M., Hatchett, B. J., Huning, L. S., Szinai, J., Tague, C., Nico, P. S., Feldman, D. R., Jones, A. D., Collins, W. D., & Kaatz, L. (2021). A low-to-no snow future and its impacts on water resources in the western United States. In *Nature Reviews Earth and Environment* (Vol. 2, Number 11, pp. 800–819). Springer Nature. https://doi.org/10.1038/s43017-021-00219-y

Smerdon, B. D. (2017). A synopsis of climate change effects on groundwater recharge. In *Journal of Hydrology* (Vol. 555, pp. 125–128). Elsevier B.V. https://doi.org/10.1016/j.jhydrol.2017.09.047

Smith, R. G., & Knight, R. (2019). Modeling Land Subsidence Using InSAR and Airborne Electromagnetic Data. *Water Resources Research*, *55*(4), 2801–2819. https://doi.org/10.1029/2018WR024185

Smith, R. G., Knight, R., Chen, J., Reeves, J. A., Zebker, H. A., Farr, T., & Liu, Z. (2017). Estimating the permanent loss of groundwater storage in the southern San Joaquin Valley, California. *Water Resources Research*, *53*(3), 2133–2148. https://doi.org/10.1002/2016WR019861

https://doi.org/10.5194/egusphere-2026-3061
Preprint. Discussion started: 11 June 2026

Somers, L. D., & McKenzie, J. M. (2020). A review of groundwater in high mountain environments. *Wiley Interdisciplinary Reviews: Water*, *7*(6), 1–27. https://doi.org/10.1002/wat2.1475

Tague, C., & Grant, G. E. (2009). Groundwater dynamics mediate low-flow response to global warming in snow-dominated alpine regions. *Water Resources Research*, *45*(7). https://doi.org/10.1029/2008WR007179

Tague, C., Grant, G., Farrell, M., Choate, J., & Jefferson, A. (2008). Deep groundwater mediates streamflow response to climate warming in the Oregon Cascades. *Climatic Change*, *86*(1–2), 189–210. https://doi.org/10.1007/s10584-007-9294-8

Talwani, P., & Acree, S. (1985). Pore pressure diffusion and the mechanism of reservoir-induced seismicity. In *Earthquake prediction* (pp. 947–965). Springer.

Tang, Q., & Oki, T. (Eds.). (2016). *Terrestrial Water Cycle and Climate Change*. John Wiley & Sons, Inc. https://doi.org/10.1002/9781118971772

Tapley, B. D., Bettadpur, S., Ries, J. C., Thompson, P. F., & Watkins, M. M. (2004). GRACE measurements of mass variability in the Earth system. *Science*, *305*(5683), 503–505. https://doi.org/10.1126/science.1099192

Tapley, B. D., Watkins, M. M., Flechtner, F., Reigber, C., Bettadpur, S., Rodell, M., Sasgen, I., Famiglietti, J. S., Landerer, F. W., Chambers, D. P., Reager, J. T., Gardner, A. S., Save, H., Ivins, E. R., Swenson, S. C., Boening, C., Dahle, C., Wiese, D. N., Dobslaw, H., … Velicogna, I. (2019). Contributions of GRACE to understanding climate change. *Nature Climate Change*, *9*(5), 358–369. https://doi.org/10.1038/s41558-019-0456-2

Torrence, C., & Compo, G. P. (1998). A practical guide to wavelet analysis [Software]. In *Bulletin of the American Meteorological Society* (Retrieved December 5, 2018.; Vol. 79, Number 1, pp. 61–78). https://doi.org/10.1175/1520-0477(1998)079<0061:APGTWA>2.0.CO;2

Urióstegui, S. H., Bibby, R. K., Esser, B. K., & Clark, J. F. (2017). Quantifying annual groundwater recharge and storage in the central Sierra Nevada using naturally occurring 35S. *Hydrological Processes*, *31*(6), 1382–1397. https://doi.org/10.1002/hyp.11112

USGS. (2021). *USGS Groundwater Data for the Nation [Dataset]*. Date Accessed: 2021-05-15. https://waterdata.usgs.gov/nwis/gw

Vasco, D. W., Kim, K., Farr, T. G., Reager, J. T., Bekaert, D., Singh, S., & Beaudoing, H. K. (2022). Using Sentinel-1 and GRACE satellite data to monitor the long- and short-term hydrological variations within the Tulare Basin , California. *Scientific Reports*, 1–14. https://doi.org/10.1038/s41598-022-07650-1

Visser, A., Moran, J. E., Singleton, M. J., & Esser, B. K. (2018). Importance of river water recharge to the San Joaquin Valley groundwater system. *Hydrological Processes*, *32*(9), 1202–1213. https://doi.org/10.1002/hyp.11468

Viswanathan, H. S., Ajo-Franklin, J., Birkholzer, J. T., Carey, J. W., Guglielmi, Y., Hyman, J. D., Karra, S., Pyrak-Nolte, L. J., Rajaram, H., Srinivasan, G., & Tartakovsky, D. M. (2022). From Fluid Flow to Coupled Processes in Fractured Rock: Recent Advances and New Frontiers. In *Reviews of Geophysics* (Vol. 60, Number 1). John Wiley and Sons Inc. https://doi.org/10.1029/2021RG000744

https://doi.org/10.5194/egusphere-2026-3061
Preprint. Discussion started: 11 June 2026

Wahi, A. K., Hogan, J. F., Ekwurzel, B., Baillie, M. N., & Eastoe, C. J. (2008). Geochemical Quantification of Semiarid Mountain Recharge. *Ground Water*, *46*(3), 414–425. https://doi.org/10.1111/j.1745-6584.2007.00413.x

Wang, H. F. (2000). *Theory of Linear Poroelasticity with Applications to Geomechanics and Hydrogeology*. Princeton Univ. Press.

Welch, L. A., & Allen, D. M. (2014). Hydraulic conductivity characteristics in mountains and implications for conceptualizing bedrock groundwater flow. *Hydrogeology Journal*, *22*(5), 1003–1026. https://doi.org/10.1007/s10040-014-1121-5

Werner, C., U. Wegmüller, T. Strozzi, & A. Wiesmann. (2000). Gamma SAR and interferometric processing software. *Proceedings of the Ers-Envisat Symposium, Gothenburg, Sweden.*

White, A. M., Gardner, W. P., Borsa, A. A., Argus, D. F., & Martens, H. R. (2022). A review of GNSS/GPS in hydrogeodesy: Hydrologic loading applications and their implications for water resource research. *Water Resources Research*. https://doi.org/10.1029/2022WR032078

Wiese, D. N., Yuan, D.-N., Boening, C., Landerer, F. W., & Watkins, M. M. (2019). *JPL GRACE and GRACE-FO Mascon Ocean, Ice, and Hydrology Equivalent Water Height CRI Filtered. Ver. RL06Mv02 [Dataset]*. PO.DAAC, CA, USA, Date Accessed 2021-12-23. https://doi.org/10.5067/TEMSC-3JC62

Wilson, J. L., & Guan, H. (2004). Mountain-block hydrology and mountain-front recharge. In *Groundwater Recharge in a Desert Environment: The Southwestern United States* (Vol. 9, pp. 113–137). American Geophysical Union. https://doi.org/10.1029/009WSA08

WMO. (2025). *State of Global Water Resources 2024*. https://doi.org/10.59327/WMO/WATER/2024

Yang, K., Rittger, K., Musselman, K. N., Bair, E. H., Dozier, J., Margulis, S. A., Painter, T. H., & Molotch, N. P. (2023). Intercomparison of snow water equivalent products in the Sierra Nevada California using airborne snow observatory data and ground observations. *Frontiers in Earth Science*, *11*. https://doi.org/10.3389/feart.2023.1106621

Zektser, I. S., & Everett, L. G. (2004). *Groundwater Resources ofthe World and Their Use* (IHP-VI Series on Groundwater No. 6). United Nations Educational, Scientific and Cultural Organization (UNESCO). https://b-ok.org/book/610713/027e58

Zhai, G., Shirzaei, M., Manga, M., & Chen, X. (2019). Pore-pressure diffusion, enhanced by poroelastic stresses, controls induced seismicity in Oklahoma. *Proceedings of the National Academy of Sciences*, 201819225. https://doi.org/10.1073/pnas.1819225116

Zheng, Y., Ross, A., Villholth, K. G., & Dillon, P. (Eds.). (2021). *Managing Aquifer Recharge: A Showcase for Resilience and Sustainability*. UNESCO. https://unesdoc.unesco.org/ark:/48223/pf0000379962